

GENERATION, CLONING, AND SMALL-SCALE EXPRESSION OF SITE-DIRECTED MUTANTS OF HEN EGG WHITE LYSOZYME IN *PICHTIA PASTORIS*

By

Nichole L. Patton

Submitted in Partial Fulfillment of the Requirements

for the Degree of

Masters of Science

in the

Chemistry

Program

YOUNGSTOWN STATE UNIVERSITY

August, 2012

Generation, Cloning, and Small-Scale Expression of Site-Directed Mutants of Hen Egg
White Lysozyme in *Pichia pastoris*

Nichole L. Patton

I hereby release this thesis to the public. I understand that this thesis will be made available from the OhioLINK ETD Center and the Maag Library Circulation Desk for public access. I also authorize the University or other individuals to make copies of this thesis as needed for scholarly research.

Signature:

Nichole Patton, Student

Date

Approvals:

Michael Serra, Ph.D., Thesis Advisor

Date

Nina Stourman, Ph.D., Committee Member

Date

David Asch, Ph.D., Committee Member

Date

Peter J. Kasvinsky, Dean of School of Graduate Studies & Research

Date

ABSTRACT

Reactive oxygen species (ROS) are compounds that are produced by the reduction of molecular oxygen; these species can generate free radicals. Metal-catalyzed oxidation systems are experimental systems that use a metal ion, such as Fe^{2+} or Cu^+ , hydrogen peroxide, and often a reducing agent to generate a free radical. The purpose of this research is to generate a suite of four site-directed mutants that were used for transformation into *Pichia pastoris* for small-scale expression of mutant lysozyme. The mutant lysozymes expressed will be used in future oxidation studies to determine the relationship between the site of oxidation and the level of protein structure. Two of the mutant genes, N103H and N77H, were created using the Polymerase Chain Reaction and the mutations were confirmed by gene sequencing. The genes were ligated into the pPICZ α A plasmid, which supported replication in both bacterial and yeast systems. The N103H gene was successfully cloned into the yeast plasmid. Two previously prepared clones in pPICZ α A, H15S and H15S+N77H, were transformed into Mach1TM-T1^R chemically competent *Escherichia coli*. Microgram amounts of the cloned plasmids were generated, and the plasmids were linearized and then transformed into *Pichia pastoris* by electroporation. The phenotype of the yeast colonies was determined and small-scale expression experiments were performed. The proteins were analyzed by SDS-PAGE and by a turbidimetric assay. One overnight growth in YPD media containing Zeocin followed by a five-day growth in YPM media with an initial concentration of 2% methanol was determined to give the highest expression of a protein that retained lysozyme activity.

ACKNOWLEDGEMENTS

I would first like to thank Dr. Michael Serra for all of his dedication to this project and for his support during my time at YSU. He was always helpful and available to answer my dilemmas and guide me through the coursework. He was also a very devoted teacher and his willingness to help his students was a great characteristic to find at YSU.

I would also like to thank my committee members Dr. Nine Stourman and Dr. David Asch for all of their time and patience with the revisions of my thesis. I appreciated how tolerant they were, even though I was not always around to answer their questions or to talk about the revisions.

I would like to thank the professors of the Chemistry and Biology Departments for all their advice and access to their equipment from time to time. Also, I owe a great deal of gratitude to the graduate students of the Chemistry Department for all their support.

I owe a final thank you to my husband Eric, both of our families, and especially to my close friends Kim and Linda for their support through all these years and for all their encouragement. I am very blessed to be surrounded by such great people in my life.

The YSU School of Graduate Studies and the YSU Chemistry Department made all this possible with their financial support and curriculum.

Table of Contents:

SECTION	PAGE#
Title Page	i
Signature Page	ii
Abstract	iii
Acknowledgements	iv
Table of Contents	v
Table of Figures	ix
Table of Equations	xiii
Table of Tables	xiv
List of Abbreviations	xv
Introduction	1
Reactive Oxygen Species	1
<i>Fenton Chemistry</i>	1
<i>Haber-Weiss Chemistry</i>	2
<i>Site-Specific Oxidation</i>	2
<i>Production of Free Radicals by Metabolism and Exercise</i>	4
Antioxidants	5
Prooxidants	7
ROS and their Role in Disease	7
<i>Iron</i>	7
<i>Copper</i>	8

<i>Cancer</i>	9
ROS Damage to DNA	10
ROS Damage to Proteins	11
<i>Damage to Amino Acid Residues</i>	11
<i>Peptide Cross-Linking</i>	13
<i>Peptide Bond Cleavage</i>	14
<i>Effects of ROS Damage on Structure and Function</i>	15
Chemical Techniques for Analysis of Oxidative Damage to Proteins	17
<i>High Performance Liquid Chromatography</i>	17
<i>Tandem Mass Spectrometry</i>	18
Biological Significance of Oxidative Damage	20
<i>In vivo versus in vitro</i>	20
<i>Diet and Oxidative Stress</i>	21
Statement of Research	22
Materials and Methods	24
Generation of Site-Directed Mutants	24
<i>Preparation of Native Lysozyme from Plasmid</i>	24
<i>Introducing the Point Mutation Using Polymerase Chain Reaction</i>	25
<i>Creating the N103H Mutation</i>	26
<i>Creating the N77H Mutation</i>	27
<i>Splicing the 5' and 3' Fragments of the Mutant Genes</i>	28
<i>Cloning the Mutant DNA Lysozyme Genes into the TOPO® Vector</i>	29
<i>Transformation of Mutant Gene in the TOPO® Plasmid into</i>	30

<i>Chemically Competent Escherichia coli</i>	
<i>Confirmation of Cloning the Mutant Genes into the TOPO® Plasmid</i>	31
<i>Sequencing Mutant Genes in the TOPO® Plasmid</i>	31
Transformation of Competent Yeast	32
<i>Preparation of Yeast Vector PICZ® for Ligation</i>	32
<i>Preparation of Mutant Genes for Ligation</i>	33
<i>Ligation of pPICZα A with the Mutant HEWL Genes</i>	34
<i>Linearization of Mutant HEWL in pPICZα A for Yeast Transformation</i>	35
<i>Sequencing of Mutants in pPICZα A</i>	36
<i>Competent Cell Generation for Electroporation</i>	36
<i>Transformation of Yeast by Mutant HEWL in pPICZα A by</i>	37
<i>Electroporation</i>	
<i>Determining the Mut Phenotype</i>	38
<i>Confirmation of Yeast Transformation by Polymerase Chain Reaction</i>	38
Expression of Mutant Proteins	40
<i>Small-Scale Expression</i>	40
Analysis of Mutant Proteins	41
<i>Turbidimetric Assay</i>	41
<i>SDS-PAGE</i>	41
Results	43
Generation of Site-Directed Mutants	43
<i>Isolation of Native Lysozyme Gene from hewl-pCR®4-TOPO®</i>	43
<i>Introducing the N103H Point Mutation</i>	43

<i>Introducing the N77H Point Mutation</i>	44
<i>Splicing the 5' and 3' Fragments of the N103H Mutation and N77H Mutation</i>	45
<i>Confirmation of the Insertion of hewl-N103H-TOPO® and hewl-N77H-TOPO®</i>	46
<i>Sequence of Mutant Genes in TOPO® Vector</i>	47
Transformation into Competent Yeast	48
<i>Preparation of Yeast Vector PICZ® for Ligation</i>	48
<i>Preparation of the Mutant Genes for Ligation into pPICZα A</i>	49
<i>Ligation of the Mutant Genes into the pPICZα A Plasmid</i>	50
<i>Sequence of Mutants in pPICZα A</i>	50
<i>Linearization of Mutant hewl DNA for Yeast Transformation</i>	52
<i>Generation of Competent Cells for Electroporation</i>	53
<i>Mutant hewl Yeast Transformation by Electroporation</i>	54
<i>Determining the Mut Phenotype</i>	56
<i>PCR Analysis</i>	56
Expression of Mutant Proteins	57
<i>Small-Scale Expression</i>	57
Analysis of Mutant Proteins	58
<i>Turbidimetric Assay</i>	58
<i>SDS-PAGE</i>	62
Discussion	65
Conclusion	71

Table of Figures

FIGURE TITLE	PAGE #
1.1 A schematic representing the mechanism of enzyme oxidation and degradation	4
1.2 A diagram showing the electron transport chain that is embedded in the inner mitochondrial membrane	5
1.3 A schematic of the homeostasis of ROS and antioxidants in normal cells and cancer cells	10
1.4 The structures of normal guanine and an altered guanine base by ROS damage	11
1.5 The mechanism of conversion of histidine to 2-oxo-histidine by MCO	13
1.6 The mechanism of formation of advanced glycation products	14
1.7 The mechanisms of peptide bond cleavage	15
1.8 A schematic displaying the timeline of how an HPLC processes data	17
1.9 A chromatogram of the separation of oxidized peptide fragment relating to the protein relaxin	18
1.10 A schematic of the representation of the chain of events for analysis by tandem mass spectrometry	19
1.11 A spectrum of the fragment derived from bovine growth hormone showing the modified histidyl residues in the fragment	20

1.12 Computer generated images of the 4 mutant HEWL proteins	23
3.1 A gel image of the digestion of <i>hewl</i> -pCR®4-TOPO® using <i>XhoI</i> and <i>EcoRI</i>	43
3.2 Gel images of the generation of the 5' and 3' fragments of the <i>hewl</i> -N103H mutation	44
3.3 Gel images of the generation of the 5' and 3' fragments of the <i>hewl</i> -N77H mutation	45
3.4 Gel images of the splicing of the 5' and 3' fragments to create a mutant lysozyme gene	46
3.5 Gel images of the double digest of the mutant <i>hewl</i> genes by <i>XhoI</i> and <i>XbaI</i>	47
3.6 Sections of the chromatogram of the <i>hewl</i> -N77H mutation	48
3.7 Section of the chromatogram of the <i>hewl</i> -N103H mutation	48
3.8 A gel image of the digestion of pPICZα A for preparation of ligation	49
3.9 Gel images of the double digestion of mutant <i>hewl</i> genes for preparation of ligation	50
3.10 Sections of the chromatogram for the <i>hewl</i> -H15S+N77H-PICZα A	51
3.11 Sections of the chromatogram of the <i>hewl</i> -H15SPICZα A	52
3.12 Gel images of the linearization of the mutant <i>hewl</i> genes for preparation of yeast transformation	53
3.13 Before and after pictures of the generation of competent	54

yeast cells using the X-33 strain of <i>Pichia pastoris</i>	
3.14 Pictures of the colonies that grew after electroporation	55
3.15 Pictures of the colonies that grew after electroporation re-streaked	55
3.16 Pictures of the determination of the Mut phenotype of the colonies that grew after electroporation	56
3.17 A gel image of the PCR results of <i>hewl</i> -H15S+N77H-PICZ α	57
A	
3.18 The standard curve of known lysozyme concentration versus the rate of cell lysis	58
3.19 A graph showing the rate of HEWL-H15S+N77H mutant protein expression over a 120-hour period	59
3.20 A graph showing the rate of HEWL-H15S mutant protein expression over a 120-hour period	59
3.21 A graph showing the difference in amount of HEWL-H15S+N77H mutant protein at hour 120	60
3.22 A graph showing the difference in amount of HEWL-H15S mutant protein at hour 48	60
3.23 A graph showing the overall comparison of growth conditions and time points for the expression of HEWL-H15S+N77H mutant protein	61
3.24 A graph showing the overall comparison of growth conditions and time points for the expression of HEWL-H15S	61

mutant protein	
3.25 A graph showing the overall comparison of mutant HEWL-H15S+N77H protein activity between the YPM growth conditions	62
3.26 An SDS-PAGE of the YPM samples at hour 72 for both HEWL mutants	63
3.27 An SDS-PAGE of the time progression of the expression of mutant protein with the initial growth in YPDZ and the 5-day growth in YPM5	63
3.28 An SDS-PAGE of the samples grown in BMM medium at hour 72	64
3.29 An SDS-PAGE of the time progression of the controls	64

Table of Equations

TITLE	PAGE #
1.1 Fenton Reaction	2
1.2 Haber-Weiss Reaction	2
2.1 The equation used to determine the concentrations of insert and vector	30

Table of Tables

TITLE	PAGE #
1.1 A list of common MCO systems	3
1.2 A list of diseases that have been linked to ROS and oxidative stress	7
1.3 Protein modification caused by metal catalyzed oxidation	12
2.2 A list of the primers used for mutation introduction	25

List of Abbreviations

μg	microgram
μL	microliter
μM	Micromolar
A	Adenine
bp	base pair
BSA	Bovine Serum Albumin
C	Cytosine
DDI	Distilled diionized water
DNA	Deoxyribonucleic Acid
EDTA	Ethylenediaminetetraacetic acid
G	Guanine
kbp	kilobase pair
mg	milligram
mL	milliliter
mM	millimolar
ng	nanogram
PAGE	Polyacrylamide gel electrophoresis
PCR	Polymerase Chain Reaction
PCR	Polymerase Chain Reaction
RNA	Ribonucleic Acid
SDS	Sodium Dodecyl Sulfate
T	Thymine

U/mL

Units per milliliter

V

Volts

CHAPTER 1: INTRODUCTION

1.1 Reactive Oxygen Species

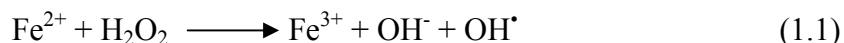
Reactive oxygen species (ROS) are compounds that either generate and/or contain a free radical (Reuter, Gupta, Chaturvedi, & Aggarwal, 2010). These free radicals evolve from reactions of electrons with molecular oxygen, O₂ (Packer, Cadenas, & Davies, 2008). ROS can react with biomolecules, like DNA, RNA, proteins, and lipids, which can lead to certain diseases, cancers, and play a major role in aging (Stadtman E. , 1990). Some of the most common ROS are the hydroxyl radical (OH[•]), the superoxide anion (O₂^{•-}), and hydrogen peroxide (H₂O₂). The hydroxyl radical is the most reactive of the free radicals. Less reactive free radicals will often react to form more reactive free radicals (Halliwell & Gutteridge, 1992).

There are antioxidant systems in place to counteract the effects of free radical damage. Antioxidants can be compounds, like ascorbic acid (Vitamin C) or glutathione, or they can be enzymes, like superoxide dismutase and catalase. An imbalance between the production of oxidants and the activity of cellular antioxidant defenses leads to oxidative stress (Halliwell, 2009). Some research being performed on free radical damage involves their role in the pathology and etiology of certain diseases, their specific interactions with biomolecules, and their reactions with antioxidants (Berlett & Stadtman, 1997) (Hofmann & Brownlee, 2004) (Reuter, Gupta, Chaturvedi, & Aggarwal, 2010).

Fenton Chemistry

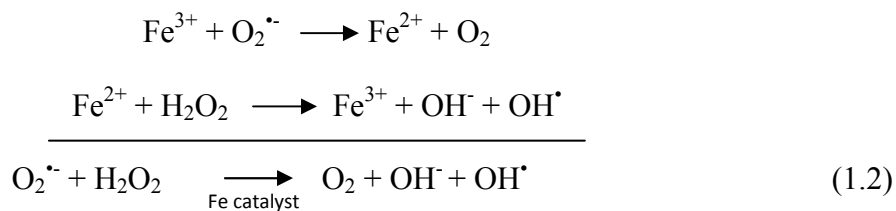
One specific example of the formation of the hydroxyl radical is the Fenton reaction, which is the reaction of the ferrous ion with hydrogen peroxide to produce the ferric ion, hydroxide, and the hydroxyl radical, Equation 1.1 (Fenton, 1894). There is

still some controversy as to whether or not it is actually the hydroxyl radical that is formed, or just some oxo-ion species. It is generally accepted at low pH, the hydroxyl radical is formed; however, at physiological pH, this reaction is much more complicated. It is believed that “crypto-OH^{*}” complexes form instead. These complexes or ferryl compounds are good oxidizers and they show the same reactivity as the hydroxyl radical (Koppenol, 1994).



Haber-Weiss Chemistry

Another common reaction known as the Haber-Weiss reaction also forms the hydroxyl radical. This reaction happens in two steps (Equation 1.2): the first reduces a metal ion to oxidize the superoxide anion to oxygen; the second will then oxidize the metal ion and reduce hydrogen peroxide to the hydroxide ion and the hydroxyl radical, (Halliwell & Gutteridge, 1992). This reaction is the basis for experimentally practical metal-catalyzed oxidation (MCO) systems used for oxidation studies.



Site-Specific Oxidation

Proteins that employ a metal ion for catalysis are more susceptible to MCO (Schoneich, 2000). Because of a protein’s tertiary or quaternary structure, a small pocket may form. If there is an amino acid residue present in that pocket that has a high affinity for a metal ion, then a reaction with oxygen will form the superoxide anion. The

exposure of superoxide anion to hydrogen peroxide will form the hydroxyl radical that will react with the surrounding residues in the pocket. This is known as a “caged” reaction. However, oxidation may still occur at positions on the protein that are not “caged,” or protected by a pocket, such as histidine that has a high affinity for copper. Therefore, the question remains: does oxidation prefers to occur due to the presence of a protective pocket to react with the amino acid residue.

When proteins are exposed to an MCO system, only a few amino acid residues are modified. Some typical modifications include the following: (1) the formation of carbonyl derivatives; (2) histidyl residues are converted to asparagine and/or aspartyl residues; (3) prolyl residues are converted to glutamyl or pyroglutamyl residues; (4) methionyl residues are converted to methionylsulfoxide residues; and (5) cysteinyl residues are converted to mixed-disulfide derivatives (Stadtman E. , 1990). This oxidation is referred to as site-specific because the OH[•] is produced at metal-ion binding site and it reacts in the immediate vicinity of its site of production.

Site-specific oxidation simply means that oxidation is contained to a localized site; this is especially true when discussing the oxidation of proteins. There are several known systems that will cause a protein to undergo oxidation. Examples of these MCO systems are in Table 1.1 (Stadtman E. , 1990). A mechanism showing the progression of ROS damage to a lysyl residue via MCO is shown in Figure 1.1.

Table 1.1: A list of common MCO systems	
Oxygen & Ferric Ion	$O_2 + Fe^{3+}$
Oxygen & Ferrous Ion	$O_2 + Fe^{2+}$
Ascorbate, Oxygen, & Ferrous Ion	$C_6H_8O_6 + O_2 + Fe^{2+}$
Hydrogen Peroxide & Ferrous Ion	$H_2O_2 + Fe^{2+}$
Ascorbate, Oxygen, & Cupric Ion	$C_6H_8O_6 + O_2 + Cu^{2+}$
Hydrogen Peroxide & Cupric Ion	$H_2O_2 + Cu^{2+}$

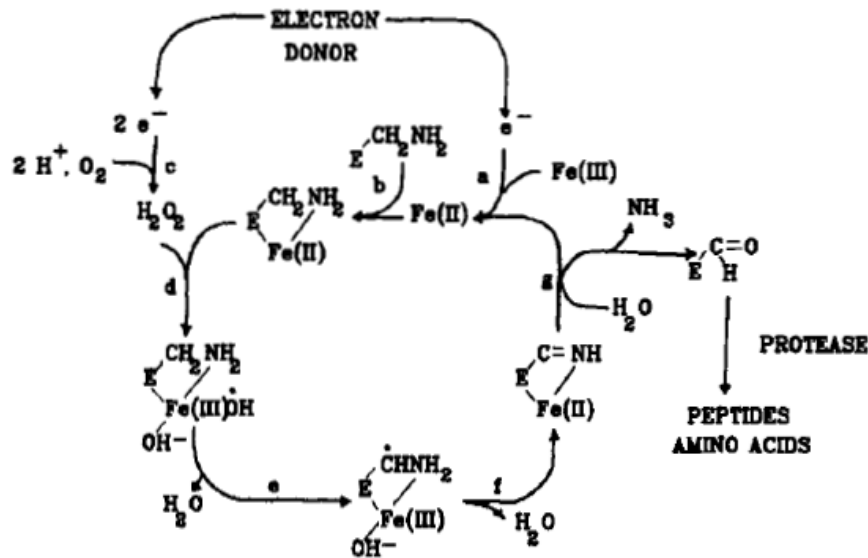


Figure 1.1: A schematic representing the mechanism of enzyme oxidation and degradation. (a) The reduction of ferric ion to ferrous ion via an electron donor. (b) The formation of an metal-enzyme complex through the lysyl residue. (c) The reduction of oxygen and free protons to form hydrogen peroxide. (d) The reaction between the complexed iron and hydrogen peroxide, forming a hydroxyl radical. (e) The rearrangement of the free radical from being complexed with iron to being complexed with the lysyl residue, and ultimately the enzyme with the loss of water. (f) The formation of a double bond via the addition of the free radical, altering the structure of the lysyl residue. (g) The deamination of the lysyl residue, which marks the protein for degradation by proteases (Stadtman & Oliver, 1991).

Production of Free Radicals by Metabolism and Exercise

Oxygen- and nitrogen-derived free radicals are generated during cellular metabolism and mitochondrial energy production and are involved in oxidative damage to cell components, regulation of signal transduction and gene expression, and activation of receptors and nuclear transcription factors (Wiseman & Halliwell, 1996). It has been found that free radicals can induce gene expression for products that act to protect against oxidative damage (Lui, Buettner, & Oberley, 2000). With normal cellular respiration, the superoxide anion can be a by-product of the electron transport chain, as pictured in Figure 1.2 (Hofmann & Brownlee, 2004).

The elevated metabolic rate that results from physical exercise will increase mitochondrial production of ROS. As O_2 consumption is increased during exercise, it

has been hypothesized that the production of superoxide anion is also increased. Other responses to exercise that can lead to oxidative stress include inflammatory responses by neutrophils and the interaction of metmyoglobin and methemoglobin with lipid peroxides (Packer, Cadenas, & Davies, 2008).

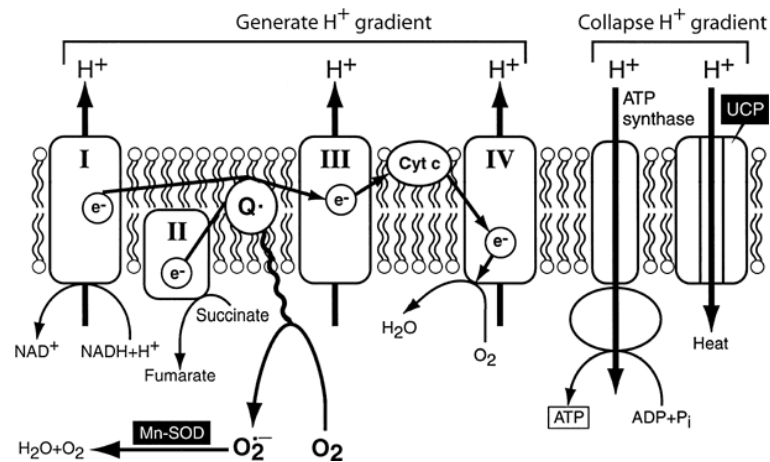


Figure 1.2: A diagram showing the electron transport chain that is embedded in the inner mitochondrial membrane. This diagram shows that a by-product of electrons “leaking” from the chain can reduce an oxygen molecule to form superoxide ion (Hofmann & Brownlee, 2004).

The difference between endurance exercise and high-intensity exercise leads to a difference in the body’s adaptive responses. With endurance training, the body is given time to adapt to the higher demand for O₂ consumption; therefore, the body is also able to adapt in order to supply the higher demand for antioxidant defenses. With high-intensity exercise, the balance between oxidants and antioxidant defenses becomes skewed due to the extremely fast and high demand of oxygen for small bursts of time (Packer, Cadenas, & Davies, 2008).

1.2: Antioxidants:

Antioxidants are molecules that eliminate ROS through protective mechanisms. Some typical antioxidant compounds include ascorbic acid (Vitamin C), glutathione, and

peroxiredoxin. Some typical antioxidant enzymes include superoxide dismutase (SOD), catalase, and thioredoxin reductase (Reuter, Gupta, Chaturvedi, & Aggarwal, 2010).

Antioxidants can be paradoxical. The assumption is that to slow aging and prevent certain diseases, an increase in consumption of antioxidants should decrease the ROS activity that plays a major role in aging and in certain diseases; however, this is not always true. There has yet to be a treatment created that is centered on the administration of antioxidants. This is due to a few reasons. First, ROS species are not directly related to the progression of a disease, it is the damage caused by ROS that has cascading effects in the development of the disease. Second, intervention trials are only performed on those patients that already have an extensive pathology due to smoking, previous heart attacks, bad lifestyle, etc. and not on patients as a preventative measure. Finally, determining the correct dosage for each patient is an intensive, time-consuming task (Halliwell, 2009).

One study by Pompella et al examined the antioxidant paradox concerning the compound glutathione. Glutathione (GSH) is a cofactor of glutathione peroxidases that reduces organic hydroperoxides created by ROS. It has been recently discovered that GSH and its catabolites will actually promote oxidative damage. GSH has been found to play a role in metal-catalyzed reactions that lead to the generation of free radicals, because its thiol groups can dissociate into the thiolate anion and donate their electrons to oxygen, forming the superoxide anion. This easily demonstrates the complexity of oxidants/antioxidants and the cell's regulation of life, proliferation, and death (Pompella, Visvikis, Paolicchi, De Tata, & Casini, 2003).

1.3: Prooxidants:

Prooxidants are compounds that stimulate oxidative damage. Prooxidants can include compounds like cytokines and growth factors, as well as processes like UV radiation, chemotherapy, and hypoxia. When there becomes an imbalance between prooxidants and antioxidants, oxidative stress occurs. This imbalance is linked to aging and inflammatory diseases. The inflammation and consequent tissue damage is what is linked to a variety of diseases. Some examples of disease linked to ROS are listed in Table 1.2 (Reuter, Gupta, Chaturvedi, & Aggarwal, 2010).

Acute Respiratory Distress Syndrome	Alzheimer
Atherosclerosis	Cancer
Cardiovascular Disease	Diabetes
Inflammation	Inflammatory Joint Disease
Neurological Disease	Obesity
Parkinson	Pulmonary Fibrosis
Rheumatoid Arthritis	Vascular Disease

1.4: ROS and their Role in Disease

Iron

Maintaining iron homeostasis is a complex process, because there are numerous proteins that not only respond to iron levels but also to iron-related conditions, such as hypoxia, anemia, and inflammation. Iron is distributed in the body in the following ways: 65% is bound to hemoglobin, 25% is bound to iron-storage proteins, and the remaining 10% is associated with other iron-containing proteins. A very minuscule percent of iron is available in the blood stream as a supply of iron, all mostly bound to transferrin. Iron complexed to transferrin ensures that iron is transferred into cells by regulatory signals so that iron is prevented from participating in the genesis of free

radicals. The uptake of iron into cells is also regulated by iron regulatory proteins (IRPs) that associate with iron-responsive elements (IREs). When there is an improper regulation of these molecules, the effects can be lethal (Jomova & Valko, 2011).

The effects of iron-mediated free radical generation and subsequent oxidative damage to biomolecules has been linked to a variety of diseases (refer to Table 2).

Elevated iron levels can predispose individuals to coronary disease and heart attacks and the iron-mediated formation of the superoxide radical and of the hydroxyl radical during disease development is a major part of the disease etiology (Jomova & Valko, 2011).

Atherosclerosis is an inflammatory condition that is characterized by the accumulation of iron and oxidized lipids in arteries as plaques. If iron is poorly ligated in the blood stream, then it is able to participate in lipid and protein peroxidation causing aggregation of oxidized tissues (Jomova & Valko, 2011). Treatment of this disease with iron-chelators will inhibit ROS generation and delay the onset of the disease. Also treatment with zinc supplements tends to reverse the extensive lipid peroxidation (Halliwell, 2009).

Copper

Copper is a trace element that is essential in metabolism because of its role as a cofactor in many enzymes and also in electron transport, the final step in cellular respiration. Copper is readily absorbed from the small intestines and is carried through the blood stream by serum ceruloplasmin or albumin to tissues or to the liver where it is imported into the liver by high-affinity copper transporters (Jomova & Valko, 2011).

Ceruloplasmin is a copper-carrying ferroxidase enzyme that carries 6-7 copper ions and accounts for 70-90% of the total copper in the bloodstream. Ceruloplasmin also has a

major role in iron metabolism, as it also transports iron from the tissues to the bloodstream by incorporating iron into transferrin (Takahashi, Ortel, & Putnam, 1983).

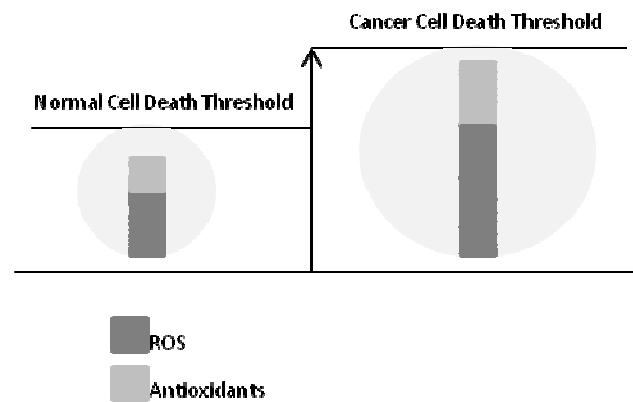
The redox capacity of copper to readily form the hydroxyl radical is thought to be the main reaction behind the neurotoxicity of β -amyloid plaques in the brain in Alzheimer's patients. Copper associates with the histidyl and tyrosinyl residues of the β -amyloid peptides and the generation of the hydroxyl radical is accompanied by the reduction of Cu (II) to Cu (I). Research has shown that there is a direct relationship between the concentration of metal ions and the toxicity of β -amyloid plaques (Jomova & Valko, 2011). Copper also exhibits an effect on the ability of the β -amyloid plaques to increase cross-linkage and aggregation in the brain (Loske, et al., 2000).

Cancer

Chronic inflammation, due to oxidative stress, has been linked to carcinogenesis, especially during cellular transformation, promotion, survival, proliferation, invasion, angiogenesis, and metastasis. During cell transformation, inflammatory cells are recruited to generate ROS, which will then cause DNA base modifications. An example of this is the activation of neutrophils and macrophages to release large quantities of superoxide, hydrogen peroxide, and the hydroxyl radical. Tumor cell survival is reliant upon the ability of ROS to increase cell proliferation, survival, and migration. ROS can also induce a variety of cellular signal transduction pathways that are involved in the transmission of inter- or intracellular information that is critical for tumor cell survival (Reuter, Gupta, Chaturvedi, & Aggarwal, 2010).

There is a fine line between the roles of ROS as an agent of oxidative damage and as an important signaling agent. ROS can signal pathways that induce cell survival and

proliferation. However, once the level of ROS overwhelms the defenses of antioxidants, cell death is triggered. Normal cells strategically balance redox homeostasis by maintaining a working level of ROS and antioxidants. In cancer cells, ROS may trigger an adaptive response that up-regulates the antioxidant capacity of the cell. This up-regulation increases the cell death threshold, allowing the damaging effects of ROS on DNA and proteins to continue, so that cancer cell survival, proliferation, and migration are promoted. Figure 1.3 displays a model of the change in ROS homeostasis between normal cells and cancer cells (Trachootham, Alexandre, & Huang, 2009).



In cancer cells, antioxidants are up-regulated to the level of healthy cells.

1.5: ROS Damage to DNA

ROS molecules can cause structural alterations in DNA through base pair mutations, rearrangements, deletions, insertions, and sequence amplifications. These changes can range from point mutations to altering the entire chromosome. One example of a lethal alteration of the entire chromosome is by the loss of the second wild-type allele of a mutated tumor-suppressor gene occurs and results in tumor progression (Wiseman & Halliwell, 1996).

The chemical reactions that alter DNA bases include oxidation, methylation, depurination, and deamination. The molecule, 8-hydroxyguanine (8-OHG), is the biomarker of ROS damage to DNA. The structure of 8-OHG is shown in Figure 1.4. This alteration also leads to the methylation of adjacent cytosine bases, linking oxidative damage to DNA to altered methylation patterns (Wiseman & Halliwell, 1996).

ROS can also damage mitochondrial DNA, which is contributory in some human diseases and in aging. Since mitochondria may be the source of intracellular production of ROS, it supports the fact that ROS damage to mitochondrial DNA is very common. It has been found that there is an increase in mitochondrial DNA damage by elevated levels of 8-OHG in Alzheimer's disease and in atherosclerotic heart tissue (Wiseman & Halliwell, 1996).

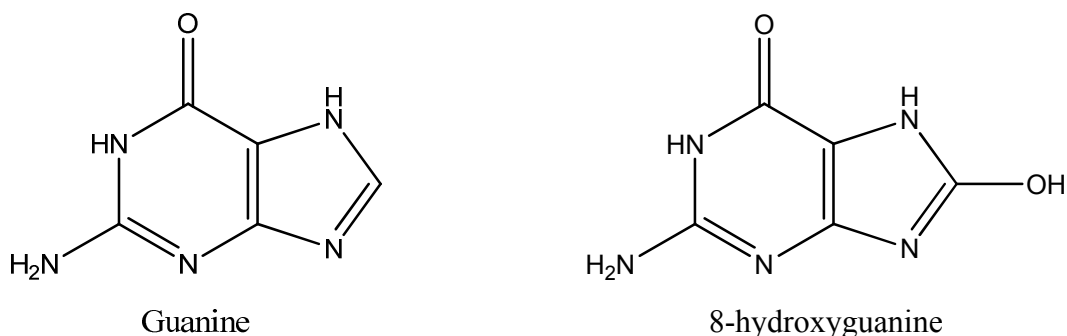


Figure 1.4: The structures of a normal guanine base (left) and an altered guanine base by ROS damage (right) (ChemDraw Ultra, 2010).

1.6: ROS Damage to Proteins:

Damage to Amino Acid Residues

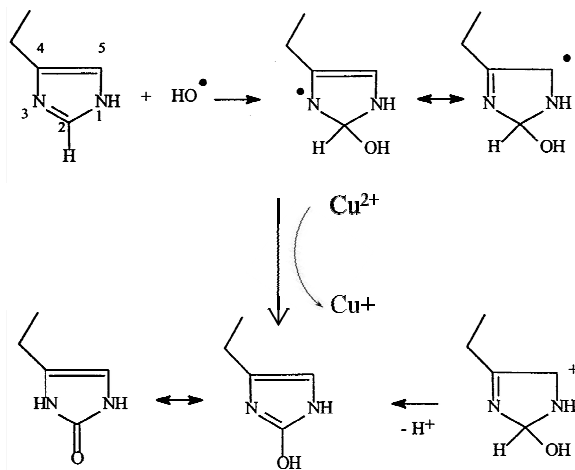
ROS damage to proteins generally occurs at specific amino acid residues. A residue that has an affinity for a transition metal ion will usually undergo oxidation by free radicals. Once a protein has undergone oxidation, it is usually “marked” for degradation by proteases. Sometimes, free radicals that are generated can cause a

cascade of alteration, leading to more widespread damage. Specific targets of ROS through MCO include histidine, proline, arginine, lysine, cysteine, and methionine.

Table 1.3 shows a list of amino acid residues and their alterations by ROS (Stadtman E. , 1990).

Table 1.3: Protein modification caused by metal catalyzed oxidation	
Amino Acid Residue	Altered Amino Acid Residue
Arginine	Glutamylsemialdehyde residues
Proline	Glutamylsemialdehyde residues Pyroglutamyl/glutamyl residues <i>Cis/trans</i> -4-hydroxy proline
Lysine	α -aminoadipylsemialdehyde residues
Histidine	Asparagine/Aspartate residues
Cysteine	Disulfide protein cross linkages Mixed disulfide proteins
Methionine	Methionylsulfoxide residues
Tyrosine	Di-tyrosinyl cross linkages

The histidyl residue can also undergo another alteration by forming 2-oxo-histidine. This alteration is an important marker for oxidative stress. The mechanism is shown in Figure 1.5. Histidine has been found to undergo other alterations depending on the protein. In human growth hormone, His21 is converted to 2-oxo-histidine after oxidative treatment. For human relaxin, the conversion of histidine to 2-oxo histidine leads to a pH-dependent, non-covalent aggregation and precipitation of a cyclic protein (Schoneich, 2000).



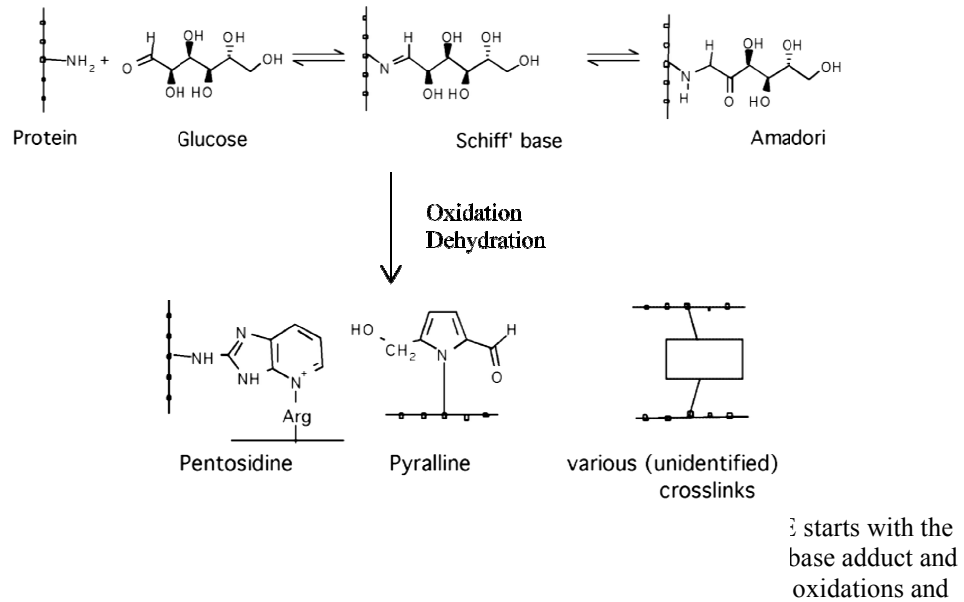
(meich, 2000).

Peptide Cross-Linking

Cross-linking simply refers to the linking of polymer chains through covalent interactions so that a network can become stronger and more insoluble. In gram positive bacteria, it is the cross linking of peptidoglycan that is responsible for the shape and insolubility of the bacteria's cell wall. The cell wall of a bacterium is very important for its survival. For instance, it is thought that the cross-linkage of peptidoglycan molecules to form a cell wall creates the site of penicillin resistance. However, not all peptide cross linkages are important for maintenance and survival. Cross linking can also occur via exposure to X-rays, causing covalent bonds to form where hydrogen bonds typically form (Dezelle & Shockman, 1975).

Alzheimer's disease (AD) is a neurodegenerative disorder that affects the synapses and the neurons and causes complete loss of memory and deductive function. A common sign of the onset of AD is the formation of amyloid deposits which are composed of the β -amyloid peptide. The insolubility of the β -amyloid plaques is caused by extensive covalent peptide cross-linking. A common mechanism for this cross linking involves the formation of "advanced glycation end products" (AGE). This mechanism is

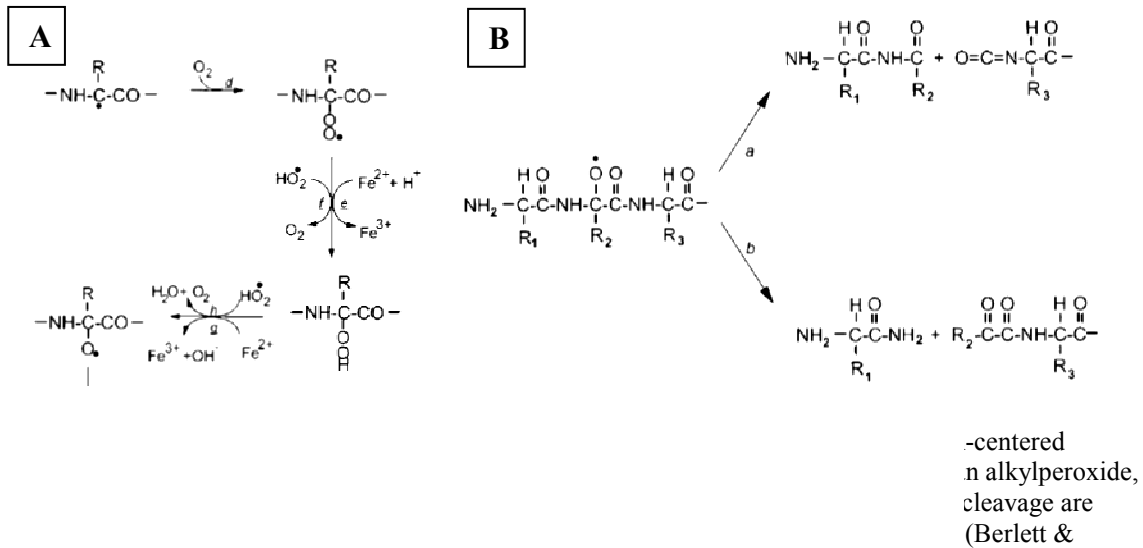
shown in Figure 1.6. Extracellular AGE formation and AD have been linked in *in vitro* studies and immunohistochemical studies. A study has also shown that trace amounts of transition metals can accelerate the formation of AGE and the subsequent covalent cross-linking of the β -amyloid peptide (Loske, et al., 2000).



Peptide Bond Cleavage

Thus far, it has been discussed how oxidation alters protein structure, whether via specific amino acid residues or via covalent cross-linking. There is also evidence of peptide bond cleavage when oxidation of the peptide backbone occurs. Cleavage of the peptide backbone usually occurs through the generation of an alkoxy radical (shown in Figure 1.7A) by two pathways. One pathway is characterized by the formation of an amide group at the C-terminal end of the peptide fragment (Figure 1.7B, reaction a) and the second pathway is characterized by the formation of a diamide structure at the C-terminal end of the peptide fragment (Figure 1.7B, reaction b). Peptide bond cleavage

can also occur by altering specific amino acids, like glutamate, aspartate, and proline (Berlett & Stadtman, 1997).



Effects of ROS Damage on Structure and Function

One study observed the effects of metal-catalyzed photooxidation of histidine in human growth hormone. Analysis of the products by anion exchange chromatography, HPLC, and MS, concluded that histidine undergoes oxidation to form a variety of products, from the addition of 1, 2, or 3 oxygen atoms. These modified histidyl residues can then be converted to asparagines or aspartate, thereby changing the primary sequence of human growth hormone. This work proposed that the stability of this protein's shelf life can be unstable, especially if divalent metal ions are present, and that the normal degradation of this protein follows the reactions of aggregation, deamidation, isomerization, and oxidation (Chang, Teshima, Milby, Gillece-Castro, & Canova-Davis, 1997).

Oxidative modification of proteins by MCO causes them to be highly susceptible to proteolytic degradation. This has been proposed to be an important step in regulating

protein turnover. Several studies have noted the proteases will prefer to degrade oxidized protein products when compared to their unoxidized counterparts and proteases will degrade oxidized protein products at a higher rate than their unoxidized counterparts. However, the structural features of the oxidized protein product that are recognized by several different proteases are poorly understood (Stadtman E. , 1990).

Oxidized protein aggregation plays a major role in the progression of aging and disease. MCO can lead to the formation of carbonyl derivatives, which will increase the density of erythrocytes and the carbonyl content of fibroblasts. This increase continues, in some instances at an exponential rate, as one ages. MCO is also an early indicator of tissue damage and the formation of carbonyl derivatives is associated with several pathological conditions, such as inflammatory diseases, atherosclerosis, neurologic disorders, and cataractogenesis (Stadtman & Oliver, 1991).

Modified lysozyme (His15) has shown an alteration of lytic activity of the enzyme. Hen egg white lysozyme (HEWL) contains one histidyl residue, located away from the active site of the enzyme. It was hypothesized that altering the histidyl residue would not affect the activity of the enzyme. The activity of the enzyme is dependent on pH and ionic strength since the lysing of cell walls is dependent on the protonation of Glu35 and the subsequent deprotonation of Asp52. It was shown that the activity of mutant HEWL was dependent on ionic strength. The mutant will have higher activity than the wild type at lower ionic strengths and the mutant will have lower activity than the wild type at higher ionic strengths. Even though the histidyl residue is far removed from the active site, it is believed that the negatively charged substrate binds near it,

changing the confirmation of the active site (Ugrankar, Krishnamoorthy, & Prabhananda, 1991).

1.7: Chemical Techniques for Analysis of Oxidative Damage to Proteins

High Performance Liquid Chromatography

High performance liquid chromatography (HPLC) is a separation technique that pushes a volume of sample through a packed column at high pressures. HPLC separates compounds in a solution based on the chemical and physical interactions of the solute with the column (stationary phase) and the solvent (mobile phase). As the compounds are separated, they pass through a detector that generates a chromatogram displaying the relative amounts of the compounds versus the time it was eluted. Figure 1.8 shows a schematic of the process (HPLC Basics). This system can be used, as an example, to separate and isolate different oxidized forms of a protein.



Figure 1.8: A schematic displaying the timeline of how an HPLC processes data. The pump pushes the solvent through the column (which is located within the injector) and is where the flow rate and flow ratios can be altered. The sample is injected into the system and is pushed through the column. Depending on how the sample interacts with the stationary and mobile phases, compounds of the sample will be flushed through a detector and a chromatogram will be created according to how much of the compound eluted and at what time (HPLC Basics).

One study done by Khossravi and Borchardt analyzed the human protein relaxin oxidized by an ascorbate/oxygen/Cu (II) system. By using this system, it was determined if oxidation of histidine caused aggregation and precipitation of the protein. The hypothesis was that the oxidation to histidine would alter the structure in such a way that it would expose the hydrophobic regions of the protein, leading to aggregation and precipitation. A hexapeptide fragment was synthesized that contained a cyclic histidyl-

containing peptide that would help validate the hypothesis. Figure 1.9 shows an overlap of three chromatograms created after oxidation at different pHs. This study concluded that the oxidation of histidine alone does not account for the aggregation and precipitation of the protein (Khosravi & Borchardt, 2000).

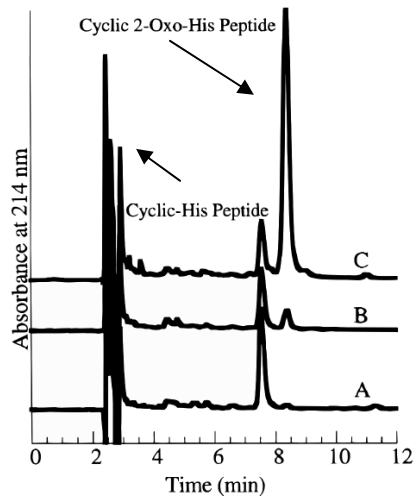
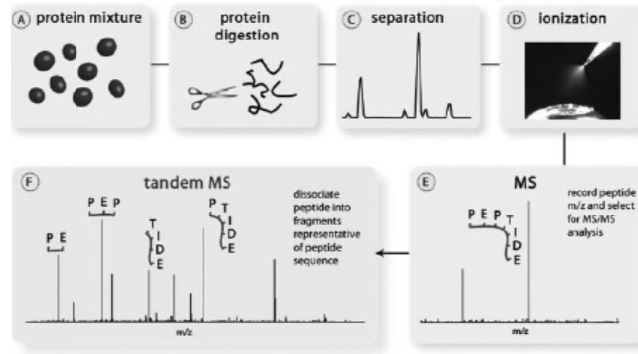


Figure 1.9: A chromatogram of the separation of oxidized peptide fragment relating to the protein relaxin. By comparing the peaks of A-C that elute between 7-9 minutes, there is a shift in the composition of the products as the pH is increased from 5.3-7.4. Each peak was analyzed by MS and the weight difference came out to be 16amu, which correlates to 1 oxygen atom being added to a histidyl residue (Khosravi & Borchardt, 2000).

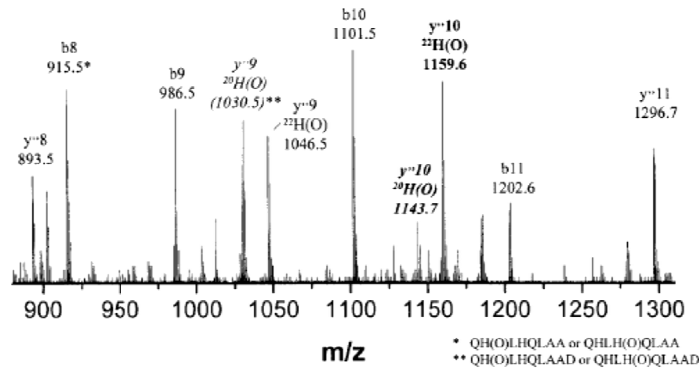
Tandem Mass Spectrometry

Tandem mass spectrometry (MS/MS) is a method used commonly to determine the primary sequence of a protein. This method works in two stages. In the first stage, the protein is digested into fragments by a protease. The fragments are then separated by reverse-phase HPLC. The second stage determines the amino acid sequence of the previously separated fragments. By looking at the difference in masses of the peaks, the specific amino acid can be determined. MS/MS can also show if there has been an alteration to a specific amino acid by noting changed from the expected mass (Coon, Syka, Shabanowitz, & Hunt, 2005). Figure 1.10 shows a timeline of the progression of MS/MS analysis.



ndem mass
and then each
2005).

One study by Hovorka et al looked at the metal-catalyzed oxidation of bovine growth hormone when exposed to an ascorbate/oxygen/Cu (II) system. This study accomplished several tasks: first, it determined the amino acids that were oxidized; second, the precise alteration of the amino acids structures was determined; and finally, the reactivity of each of those amino acids was determined. The authors found that there were two fragments that contained altered structures of histidine by the addition of 16 amu, which correlated to one oxygen atom. Out of the three histidyl residues within those two fragments, one of those was found to be much more susceptible to oxidation than the other two residues. Figure 1.11 shows a spectrum of one of the fragments that contained two altered histidyl residues by the increase of mass (Hovorka, Williams, & Schoneich, 2002).



; the modified

1.8: Biological Significance of Oxidative Damage

In vivo versus in vitro

The cell contains many organelles, each of which carries out specific processes that are essential for life. Chemical reactions and biological interactions within the confines of an organism depend on the structure of each biomolecule and its subcellular localization. By removing these complications and focusing on a purified substance, extra reactions and interactions will be prevented and the results can be more easily analyzed. However, without carrying out research in the organism as a whole, the results of the studies may be skewed or even incorrect. Most studies employ both types of research so to establish a concrete understanding of the results, to confirm results, or to make parts of the research easier and simpler by choosing either *in vivo* or *in vitro* to accomplish a part of a protocol (Nasr, 1995). How diet changes affect the amount of oxidative damage to biomolecules in one's old age versus direct exposure of antioxidants to oxidatively-damaged biomolecules in a test tube is a good illustration between *in vivo* and *in vitro* testing.

Diet and Oxidative Stress

Our diet greatly influences our overall health. With a well balanced diet, our cells and tissues have a ready-supply of antioxidants to combat the destructiveness of free radicals. However, the overall lifestyle of the population has affected our diets in a negative way, such that there is a much less intake of fruits and vegetables. Fruits and vegetables contain essential compounds that act as important antioxidants. Some examples include tomatoes, citrus fruits, tea, and carrots. Tomatoes contain lycopene, carrots contain β -carotene, citrus fruits contain phytochemicals, and tea contains catechin. Antioxidant mechanisms involving lycopene, for example, function by interfering with growth factor receptor signaling and cell cycle progression in human cancer cell growth, and an up-regulation of the connexin 43 gene, which is responsible for direct intercellular gap junctional communication that decreases proliferation in human cancer cells (Heber & Lu, 2002).

A study by Krajcovicova-Kudlackova et al compared the oxidative damage to DNA between young and old, vegetarian and non-vegetarian women. These women were of average weight and BMI (body mass index) and were all non-smokers, eliminating other common conditions that affect oxidation. The study measured oxidative damage by the amount of DNA breaks, DNA breaks with oxidized purines, DNA breaks with oxidized pyrimidines, conjugated dienes of fatty acids, protein carbonyls, and the amount of Vitamin C, A, E, and β -carotene serum levels. In the younger subjects, there was no significant difference in oxidative damage or serum levels between the vegetarians and non-vegetarians. In the older subjects, there was a significant decrease of oxidative damage and significant increase in vitamin serum levels

in vegetarians as compared to non-vegetarians. There was also a significant increase in oxidative damage and decrease in vitamin serum levels between the younger, non-vegetarians and the older, non-vegetarians. There was little difference in oxidative damage and vitamin serum levels of the vegetarians, no matter the age. In conclusion, a lifestyle that includes a diet rich in fruits and vegetables will, over time, decrease the oxidation of biomolecules and increase the serum levels of antioxidants (Krajcovicova-Kudlackova, Valachovicova, Paukova, & Dusinska, 2008). This situation could lead to a decreased risk of those diseases listed in Table 2. However, because of the complexity of the mechanisms of those diseases, a direct relationship between a healthier lifestyle and decreased risk is difficult to confirm.

1.9: Statement of Research

The overall purpose of this project is to observe the site-specificity of oxidation of hen egg white lysozyme (HEWL) using MCO systems. In order to accomplish this, a series of three site-directed mutant proteins, N77H, N103H, and H15S, and one double mutant protein, H15S + N77H, were created. Computer-generated images of the mutants are shown in Figure 1.12 (Kelley & Sternbery, 2009). The mutations that replaced amino acids with a histidyl residue were used because of histidine's affinity for copper (Cu (II)). The residues at positions 77 and 103 are found on the surface of the protein while the residue at 15 is found within a protective pocket (different from the binding pocket). In the native protein, position 15 contains the only histidyl residue in HEWL. By changing two surface amino acids to histidyl residues, a new binding site for copper will be created. By changing the residue at position 15, the protective pocket will lack histidine and possibly not bind a copper ion. The purpose of the double mutant is to determine if

the site of copper binding can be changed. This suite of mutants creates a competitive study between the two types of binding sites—one in a protective pocket and another exposed on the protein’s surface.

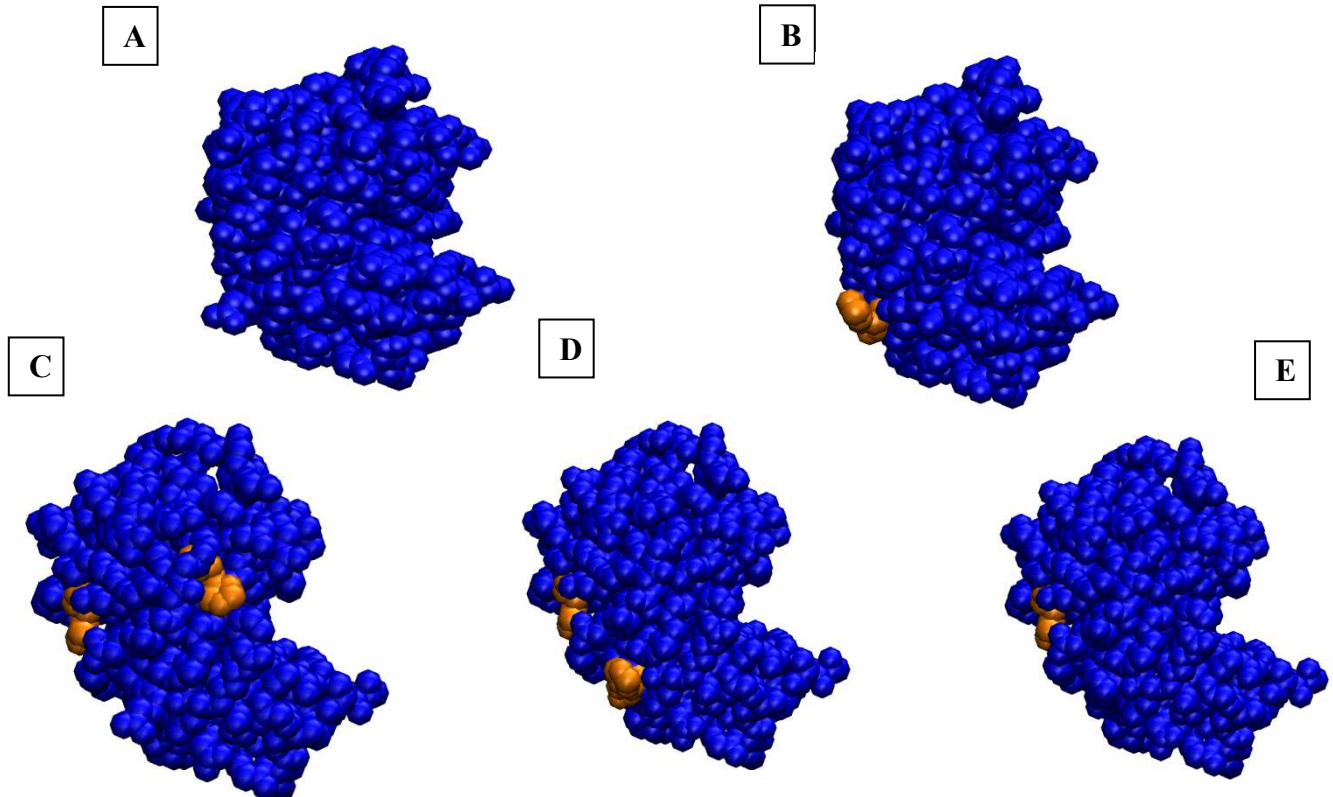


Figure 1.12: Computer generated images of the 4 mutant HEWL proteins. The orange residues show the position of the histidyl residues for each mutant. (A) H15S creates a mutation that removes the histidyl residue from the pocket. (B) H15S+N77H is a double mutant that moves the histidyl residue from the pocket to the exterior of the protein. (C&D) N103H and N77H are mutations that insert a histidyl residue on the exterior of the protein, creating a competition for Cu(II) binding (E) Native HEW lysozyme contains one histidyl residue in a protective pocket (VMD, 2010).

This research focused on two subprojects. The first was creating two of the mutants (N103H and N77H) from the native lysozyme using the polymerase chain reaction (PCR). After the mutant gene was created, it was ligated into a sequencing plasmid and later sequenced to ensure that the position of the mutation was correct and also to ensure the gene inserted correctly into the plasmid. The second part of this research was to transform the plasmids containing genes for the expression of the other two mutants (H15S and H15S+N77H) into the yeast system *Pichia pastoris* and then determine the optimal conditions for extracellular expression of the mutant lysozymes.

Chapter 2: Materials and Methods

2.1: Generation of Site-Directed Mutants

Preparation of Native Lysozyme from Plasmid

The native lysozyme gene from hen egg white (HEW) was digested out of a sequencing plasmid to serve as a template for the point mutations. A volume of 40 μL of HEWL in pCR4®TOPO in *E. coli* were plated on Luria-Bertini (LB) medium (1.0% tryptone, 0.5% yeast extract, and 1.0% NaCl, 1.5% agar, pH 7.0) plates with ampicillin (0.1 mg/mL) and were grown overnight at 37 °C (colonies were previously made by Michael Serra, Chemistry Department, Youngstown State University). Selected colonies were then inoculated in 2 mL LB medium containing ampicillin and grown overnight at 37 °C in a shaking incubator at 225 rpm. The DNA was isolated using the QIAprep® Spin Miniprep Kit from *QIAGEN*.

The isolated plasmid was then digested using 2 restriction enzymes, *XbaI* and *EcoRI* from *New England Biolabs*. The digestion mixture was prepared as follows: 10-12.5 μL of 40-120 ng/ μL HEWL DNA in pCR®4-TOPO®, 5 μL of 10 mg/mL BSA, 5 μL 10X NE Buffer 4, 2 μL of 20,000 U/mL *EcoRI*, and 2 μL of 20,000 U/mL *XbaI*. The volume was brought up to 50 μL with sterile water. The reaction was incubated for 2 hours at 37 °C and was then loaded on a 1% agarose gel and run at 85V for 52 minutes. The gel was soaked in a solution of 5 $\mu\text{g}/\text{mL}$ ethidium bromide in 1 X TAE buffer for 15 minutes and visualized using the Eagle Eye II Stratagene system. The band corresponding to the gene (400 bp) was cut out of the gel and the DNA was isolated using the Cyclo-Pure™ Agarose Gel Extraction Kit from *AMRESCO*.

Introducing the Point Mutation Using the Polymerase Chain Reaction

The method used for creating the mutant DNA sequences is known as the overlap extension method, which uses PCR to introduce the point mutation. The DNA is assembled in two parts, a 3' fragment and a 5' fragment about the point mutation. Once those 2 parts have been amplified by PCR and isolated, they are then annealed together to create a gene of normal size (400 bp). The primers used are listed in Table 2.1.

Table 2.1: A list of the primers used for mutation introduction	
5'ExLyso	5' CCCGC <u>CTCGAG</u> AAAAGA <u>AAAGTCTTT</u> 3' XhoI Lys Val Phe (1 st three codons of lysozyme)
LyzR	5' <u>CTCTAGA</u> GCCGGCCT 3' XbaI
N103HR	5' TTCATGCC <u>GTG</u> TCCATCGCT 3' N103H
N103HF	5' AGCGATGGAC <u>CAC</u> GGCATGAA 3' N103H
N2HF	5' AACCTGTGC <u>CAC</u> ATCCCGTGC 3' N77H
N2HR	5' GCACGGGAT <u>GTG</u> GCACAGGTT 3' N77H

To introduce the mutation, specialized primers that contain the base pair mutation were utilized. Together, N103HR and 5'ExLyso generated the 5' fragment of the gene (~300 bp) and N103HF and LyzR generated the 3' fragment of the gene (~100 bp). The mutation is introduced within the sequence of N103HF. This same concept holds true for the N77H mutation, except for the use of 2 different primers, N2HF and N2HR. The 5'ExLyso primer also contains an *XhoI* restriction enzyme site that places the gene within the correct reading frame of a signal sequence for extracellular expression. All primers were prepared by *Integrated DNA Technologies*.

Creating the N103H Mutation

The PCR protocol for creating the 5' fragment of N103H mutant HEWL was as follows: 6.5 μL of 10 ng/ μL HEWL DNA, 7.5 μL of 25 mM MgCl_2 , 2.5 μL of 10 mM dNTPs, 5 μL 10X Thermopol Buffer, 2.5 μL of 10 μM 5'ExLyso, 2.5 μL of 10 μM N103HR, 2.5 μL of 0.25 U/mL *Vent Polymerase* (*New England Biolabs*). The volume brought up to 50 μL with sterile water. The PCR reaction was performed with a thermocycler (Techgene version 10.19) using the following program: an initial heat denaturation at 95 $^\circ\text{C}$ for 2 minutes, then a loop repeated 30 times consisting of heat denaturation at 95 $^\circ\text{C}$ for 1 minute, annealing at 54 $^\circ\text{C}$ for 30 seconds, and extension at 72 $^\circ\text{C}$ for 1 minute. The program ended with a final extension at 72 $^\circ\text{C}$ for 25 minutes. The reaction was loaded on a 1% agarose gel and was run at 85 V for 50-55 minutes. The gel was soaked in a solution of 5 $\mu\text{g}/\text{mL}$ ethidium bromide in 1 X TAE buffer for 15 minutes and visualized using the Eagle Eye II Stratagene system. The band was cut out and the DNA extracted by the Cyclo-Pure™ Agarose Gel Extraction Kit from *AMRESCO* (*Producing PCR Products*, 2002).

The PCR protocol for creating the 3' fragment of N103H mutant HEWL was as follows: 6.5 μL of 10 ng/ μL HEWL DNA, 5 μL of 25 mM MgCl_2 , 2.5 μL of 10 mM dNTPs, 10 μL 10X Thermopol Buffer, 2.5 μL of 10 μM LyzR, 2.5 μL of 10 μM N103HF, 2.5 μL of 0.25 U/mL *Vent Polymerase* (*New England Biolabs*). The volume was brought up to 50 μL with sterile water. The PCR reaction was performed with a thermocycler (Techgene version 10.19) and the program was as follows: an initial heat denaturation at 95 $^\circ\text{C}$ for 2 minutes, then a loop repeated 30 times consisting of heat denaturation at 95 $^\circ\text{C}$ for 1 minute, annealing at 55 $^\circ\text{C}$ for 30 seconds, and extension at 72

°C for 1 minute. The program ended with a final extension at 72 °C for 25 minutes. The reaction was loaded on a 1% agarose gel and was run at 85 V for 50-55 minutes. The gel was soaked in a solution of 5 µg/mL ethidium bromide in 1 X TAE buffer for 15 minutes and visualized using the Eagle Eye II Stratagene system. The band was cut out and the DNA extracted by the Cyclo-Pure™ Agarose Gel Extraction Kit from *AMRESCO* (Producing PCR Products, 2002).

Creating the N77H mutation

The PCR protocol for creating the 5' fragment of the N77H mutant HEWL was as follows: 6.5 µL of 10 ng/µL HEWL DNA, 5 µL of 25 mM MgCl₂, 2.5 µL of 10 mM dNTPs, 10 µL 10X Thermopol Buffer, 2.5 µL of 10 µM 5'ExLyso, 2.5 µL of 10 µM N2HR, 2.5 µL of 0.25 U/mL *Vent Polymerase* (*New England Biolabs*). The volume was brought up to 50 µL with sterile water. The PCR reaction was performed with a thermocycler (Techgene version 10.19) and the program was as follows: an initial heat denaturation at 95 °C for 2 minutes, then a loop repeated 30 times consisting of heat denaturation at 95 °C for 1 minute, annealing at 55 °C for 30 seconds, and extension at 72 °C for 1 minute. The program ended with a final extension at 72 °C for 25 minutes. The reaction was loaded on a 1% agarose gel and was run at 85 V for 50-55 minutes. The gel was soaked in a solution of 5 µg/mL ethidium bromide in 1 X TAE buffer for 15 minutes and visualized using the Eagle Eye II Stratagene system. The band was cut out and the DNA extracted by the Cyclo-Pure™ Agarose Gel Extraction Kit from *AMRESCO* (Producing PCR Products, 2002).

The PCR protocol for creating the 3' fragment of N77H mutant HEWL was as follows: 6.5 µL of 10 ng/µL HEWL DNA, 5 µL of 25 mM MgCl₂, 2.5 µL of 10 mM

dNTPs, 10 μ L 10X Thermopol Buffer, 2.5 μ L of 10 μ M LyrR, 2.5 μ L of 10 μ M N2HF, 2.5 μ L of 0.25 U/mL *Vent Polymerase* (*New England Biolabs*). The volume was brought up to 50 μ L with sterile water. The PCR reaction was performed with a thermocycler (Techgene version 10.19) and the program was as follows: an initial heat denaturation at 95 $^{\circ}$ C for 2 minutes, then a loop repeated 30 times consisting of heat denaturation at 95 $^{\circ}$ C for 1 minute, annealing at 54 $^{\circ}$ C for 30 seconds, and extension at 72 $^{\circ}$ C for 1 minute. The program ended with a final extension at 72 $^{\circ}$ C for 25 minutes. The reaction was loaded on a 1% agarose gel and was run at 85 V for 50-55 minutes. The gel was soaked in a solution of 5 μ g/mL ethidium bromide in 1 X TAE buffer for 15 minutes and visualized using the Eagle Eye II Stratagene system. The band was cut out and the DNA extracted by the Cyclo-Pure™ Agarose Gel Extraction Kit from *AMRESCO* (Producing PCR Products, 2002).

Splicing the 5' and 3' Fragments of the Mutant Genes

The 5' and 3' fragments of each site-directed mutant were spliced together to create the mutant gene. The PCR protocol for splicing the 5' and 3' fragments of the N103H mutation was as follows: 10 μ L of 2.0 ng/ μ L 5' fragment DNA template, 10 μ L of 2.0 ng/ μ L 3' fragment template, 2.5 μ L of 10 μ M 5'ExLyso primer, 2.5 μ L of 10 μ M LyrR primer, and 25 μ L of 2X Green Master Mix (*Promega*). The PCR reaction was performed with a thermocycler (Techgene version 10.19) and the program was as follows: an initial heat denaturation at 95 $^{\circ}$ C for 2 minutes, then a loop repeated 30 times consisting of heat denaturation at 95 $^{\circ}$ C for 30 seconds, annealing at 58 $^{\circ}$ C for 45 seconds, and extension at 72 $^{\circ}$ C for 30 seconds. The program ended with a final extension at 72 $^{\circ}$ C for 15 minutes. The reaction was loaded on a 1% agarose gel and was

run at 85 V for 50-55 minutes. The gel was soaked in a solution of 5 µg/mL ethidium bromide in 1 X TAE buffer for 15 minutes and visualized using the Eagle Eye II Stratagene system. The band was cut out and the DNA extracted by the Cyclo-Pure™ Agarose Gel Extraction Kit from *AMRESCO* (Producing PCR Products, 2002).

The PCR protocol for splicing the 5' and 3' fragments of the N77H mutation was as follows: 10 µL of 2.0 ng/µL 5' fragment DNA template, 10 µL of 2.0 ng/µL 3' fragment template, 2.5 µL of 10 µM 5'ExLyso primer, 2.5 µL of 10 µM LyzR primer, and 25 µL of 2X Green Master Mix (*Promega*). The PCR reaction was done with a thermocycler (Techgene version 10.19) and the program was as follows: an initial heat denaturation at 95 °C for 2 minutes, then a loop repeated 30 times consisting of heat denaturation at 95 °C for 30 seconds, annealing at 58 °C for 45 seconds, and extension at 72 °C for 30 seconds. The program ended with a final extension at 72 °C for 15 minutes. The reaction was loaded on a 1% agarose gel and was run at 85 V for 50-55 minutes. The gel was soaked in a solution of 5 µg/mL ethidium bromide in 1 X TAE buffer for 15 minutes and visualized using the Eagle Eye II Stratagene system. The band was cut out and the DNA extracted by the Cyclo-Pure™ Agarose Gel Extraction Kit from *AMRESCO* (Producing PCR Products, 2002).

Cloning the Mutant DNA Lysozyme Genes into the TOPO® Vector

Now that the mutant gene was available, one easy way to replicate it was to use a bacterial system. However, before the DNA can be transformed into bacteria, it must first be cloned into a plasmid that will be supported by a bacterial system. The plasmid of choice was the TOPO® vector, specifically pCR®4-TOPO®, because of its ease for sequencing. The cloning reaction for the N103H gene and the N77H gene was 1 µL of

2.0 ng/μL DNA, 1 μL of a salt solution (1.2 M NaCl, 0.06 M MgCl₂), 2 μL of sterile, nuclease-free water, and 1 μL of 10 ng/μL TOPO® vector from the TOPO TA Cloning® Kit for Sequencing, provided by *Invitrogen* (Setting up the TOPO Cloning Reaction, 2002). These concentrations were calculated with a 1:1 ratio of vector to insert and by the use of Equation 2.1. The reaction was allowed to incubate anywhere from 30 seconds to 30 minutes before transformation.

$$\text{ng insert} = \frac{\text{ng vector} \times \text{kbp insert}}{\text{kbp vector}} * \text{molar ratio} \frac{\text{insert}}{\text{vector}}$$

Equation 2.1: The equation used to determine the concentrations of insert (gene) and of vector. If one were to increase the insert: vector ratio, one would multiply by that ratio (Oswald, 2007).

Transformation of the Mutant Gene in the TOPO® Plasmid into Chemically Competent Escherichia coli

The cloned TOPO® plasmids that contained the mutant genes were transformed into a bacterial host. The bacteria chosen were the One Shot® Mach1™-T1® Phage Resistant Chemically Competent *E. coli* (*Invitrogen*). A volume of 2 μL from the cloning reaction described in the previous section were added to 50 μL of chemically competent bacterial cells and mixed gently by flicking. The tube was then incubated on ice for 5-30 minutes. The cells were heat-shocked at 42 °C for 30 seconds and then the tube was immediately transferred to ice. A volume of 250 μL of SOC media from *Invitrogen* (Super Optimal Media with Catabolite Repression; SOC is a nutrient-rich media for bacteria) was added to the tube and the tube was incubated at 37 °C for 1 hour with horizontal shaking at 200 rpm. Different volumes of the reaction, from 10 μL to 50 μL (with all volumes brought up to 50 μL with SOC media) were plated on LB medium containing 0.1 mg/mL ampicillin. The plates were incubated overnight at 37 °C. After

one overnight growth, a few colonies were selected and re-streaked on fresh LB medium plates with 0.1 mg/mL ampicillin and incubated overnight at 37 °C. One of each colony from the second overnight growth was used to inoculate 2 mL of LB medium with 0.1 mg/mL ampicillin and were incubated overnight at 37 °C with shaking at 225 rpm. The cells were then pelleted and the plasmid was extracted using the QIAprep® Spin Miniprep Kit (*QIAGEN*). The DNA was re-suspended in 50 µL of sterile water (Transforming One Shot Competent Cells, 2002).

Confirmation of Cloning the Mutant Genes into the TOPO® Plasmid

In order to confirm that the cloning reaction was successful, the DNA was digested using two restriction enzymes, *XhoI* and *XbaI* from *New England Biolabs*. The digestion mixture was prepared as follows: 4 µL of 40-80 ng/µL of the N103H gene or the N77H gene, 2 µL of 10X NE Buffer 4, 2 µL of 10 mg/mL BSA, 1 µL of 20,000 U/mL *XhoI*, and 1 µL of 20,000 U/mL *XbaI*. The reaction was brought up to 20 µL using sterile water. The solution was incubated for 2 hours at 37 °C. The reaction was loaded on a 1% agarose gel and was run at 85 V for 50-55 minutes. The gel was soaked in a solution of 5 µg/mL ethidium bromide in 1 X TAE buffer for 15 minutes and visualized using the Eagle Eye II Stratagene system.

Sequencing Mutant Genes in the TOPO® Plasmid

The genes were sequenced using the GenomeLab™ Dye Terminator Cycle Sequencing with Quick Start Kit (*Beckman Coulter*). For a sequencing reaction, two protocols were used: 2-5 µL of a 40-80 ng/µL N103H gene or N77H gene in pCR®4-TOPO® for each reaction (for sequencing, 130-260 ng are needed), 2 µL of 16 µM of T3 primer for one reaction and 2 µL of 16 µM T7 primer for the second reaction, 8 µL of

DTCS Master Mix for each reaction, and each reaction was brought up to 20 μL using sterile water. The order the reagents were added was crucial; the order was water, DNA, primer, and DTCS Master Mix. The sequencing reaction was prepared by PCR using a thermocycler (Techgene version 10.19). The program was as follows: an initial heat denaturation at 96 $^{\circ}\text{C}$ for 2 minutes, then a loop repeated 30 times consisting of heat denaturation at 96 $^{\circ}\text{C}$ for 20 seconds, annealing at 48 $^{\circ}\text{C}$ for 20 seconds, and extension at 60 $^{\circ}\text{C}$ for 4 minutes. Once the reaction was completed, 5 μL of a stop solution was added to the tube. The stop solution was composed of 2 μL of 3.0 M NaCH_3COO pH 5.2, 2 μL of 100 mM Na_2EDTA , and 1 μL of 20 mg/mL glycogen. Then 60 μL of ice cold 95% ethanol was added and the tube was flicked to mix the solutions. The tube was then centrifuged at 13,000 rpm for 15 minutes at 4 $^{\circ}\text{C}$. The supernatant was removed using a mechanical pipette. The pellet of DNA (which was translucent) was washed with 200 μL of ice cold 70% ethanol and centrifuged for 2-5 minutes at 13,000 rpm at 4 $^{\circ}\text{C}$. The supernatant was removed and the wash was repeated. A final drying using a CentriVap DNA Concentrator (*LABCONCO*) was performed at 37 $^{\circ}\text{C}$ for 15-30 minutes. The sample was re-suspended in 40 μL of the sample loading buffer (GenomeLab DTCS with Quick Start Kit, 2007). The samples were using a Beckman Coulter CEQTM 2000 DNA Sequencer by Mr. Julio Budde (Biology Department, Youngstown State University). The generated computer files were analyzed using chromas[®] software.

2.2: Transformation of Competent Yeast

Preparation of Yeast Vector PICZ[®] for Ligation

Once the N103H and N77H mutants had been confirmed by double digestion and sequencing, the genes were ligated into another plasmid. The plasmid chosen was the

pPICZ α A plasmid from *Invitrogen*. This plasmid confers Zeocin resistance as a selective marker. It also contains an α -factor signal sequence for extracellular expression of the gene product. Finally, the plasmid is designed for over-expression of the cloned gene when placed behind the alcohol oxidase gene promoter and methanol is the only carbon source available.

In order to insert the mutant gene, the PICZ α plasmid was digested using two restriction enzymes, *XhoI* and *XbaI*. The digestion reaction was as follows: 4 μ L of pPICZ α A (provided by *Invitrogen*), 5 μ L 10 mg/mL BSA, 5 μ L 10X NE Buffer 4, 2.5 μ L of 20,000 U/mL *XhoI*, and 2.5 μ L of 20,000 U/mL *XbaI*. The volume was brought up to 50 μ L using sterile water. The reaction was incubated at 37 °C for 2 hours. The reaction was loaded on a 1% agarose gel and was run at 85 V for 50-55 minutes. The gel was soaked in a solution of 5 μ g/mL ethidium bromide in 1 X TAE buffer for 15 minutes and visualized using the Eagle Eye II Stratagene system. The DNA was isolated from the reaction using the Cyclo-Prep 2 in 1 Isolation Kit from *AMRESCO*.

Preparation of Mutant Genes for Ligation

The genes were digested out of pCR α 4-TOPO α so that they could be inserted into the pPICZ α A plasmid. The digestion mixture was prepared as follows: a concentrated amount (at least 2 μ g) of the N103H gene or the N77H gene (prepared by drying down the isolated DNA using a CentriVap DNA Concentrator (*LABCONCO*) at 37 °C for 45 minutes), 5 μ L 10 mg/mL BSA, 5 μ L 10X NE Buffer 4, 2.5 μ L of 20,000 U/mL *XhoI* and 2.5 μ L of 20,000 U/mL *XbaI*. The final volume was brought up to 50 μ L using sterile water. The reaction was incubated at 37 °C for 2 hours. The reaction was loaded on a 1% agarose gel and was run at 85 V for 50-55 minutes. The gel was soaked

in a solution of 5 µg/mL ethidium bromide in 1 X TAE buffer for 15 minutes and visualized using the Eagle Eye II Stratagene system. The DNA was extracted from the gel using the Cyclo-Pure™ Agarose Gel Extraction Kit from *AMRESCO*.

Ligation of pPICZα A with the Mutant HEWL Genes

The genes were cloned into the pPICZα A plasmid using the Quick Ligation™ protocol from *New England Biolabs*. The amount of insert needed was determined using Equation 2.1. An amount of 50 ng of vector was ligated with the gene insert in a 3:1 insert: vector molar ratio. The ligation mixture was prepared as follows: 1.6 µL of 10 ng/µL N103H or N77H gene, 10 µL Quick Ligation Buffer™, 1 µL of 50 ng/µL pPICZα A, 1 µL of Quick Ligase™, and the volume was brought up to 21 µL using sterile water. The 5 µL of the reaction was incubated at room temperature for 5 minutes (Quick Ligation Protocol). Then the reaction was transformed into One Shot® Mach1™ Chemically Competent *E. coli* and spread on low-salt LB (1.0% tryptone, 0.5% yeast extract, and 0.5% NaCl, 1.5% agar, pH 7.5) with 100 µg/mL Zeocin plates that were then incubated overnight at 37 °C. Two colonies of the N103H mutant in pPICZα A were re-streaked and incubated for a second night at 37 °C. Finally, one colony from each plate was inoculated into 2 mL of low salt LB broth and grown overnight with shaking at 225 rpm at 37 °C. Several efforts to ligate N77H into in pPICZα A were unsuccessful. The focus was shifted from the N103H and N77H mutant to the H15S and H15S+N77H mutants. These mutants were already ligated into the pPICZα A plasmid by Michael Serra (Chemistry Department, Youngstown State University) and ready for yeast transformation.

Linearization of Mutant HEWL in pPICZ α A for Yeast Transformation

The DNA was linearized for yeast transformation by digestion with the restriction enzyme, *BstXI* (New England Biolabs). A colony of transformed Mach1™ *E. coli* was chosen and used to inoculate 2 mL of low salt LB broth containing 100 $\mu\text{g/mL}$ Zeocin. The broth was shaken at 225 rpm for 8 hours at 37 °C. A volume of 100 μL of the overnight growth was used to inoculate 100 mL of low salt LB broth containing 100 $\mu\text{g/mL}$ Zeocin. The broth was shaken at 225 rpm for 12-16 hours at 37 °C. The DNA was isolated according to the protocol provided by *QIAGEN* in the *QIAGEN*® Plasmid Midi Kit. Approximately 400 μg of DNA was isolated.

The linearization mixture was prepared as follows: 50 μL of 40 ng/ μL H15S or H15S+N77H mutant in pPICZ α A, 20 μL 10mg/mL BSA, 20 μL 10X NE Buffer 3, and 10 μL of 10,000 U/mL *BstXI*. The volume was brought up to 200 μL using sterile water. The reaction was incubated at 37 °C for 1.5 hours. The reaction was loaded on a 1% agarose gel and was run at 85 V for 50-55 minutes. The gel was soaked in a solution of 5 $\mu\text{g/mL}$ ethidium bromide in 1 X TAE buffer for 15 minutes and visualized using the Eagle Eye II Stratagene system (Preparation of Transforming DNA).

The pPICZ α A plasmid was also linearized for yeast transformation. The linearization mixture was prepared as follows: 40 μL 40 ng/ μL of pPICZ α A DNA, 20 μL 10mg/mL BSA, 20 μL 10X NE Buffer 3, 10 μL of 20,000 U/mL *XhoI*, and 10 μL of 20,000 U/mL *XbaI*. The volume was brought up to 200 μL using sterile water. The reaction was incubated at 37 °C for 2 hours. The reaction was loaded on a 1% agarose gel and was run at 85 V for 50-55 minutes. The gel was soaked in a solution of 5 $\mu\text{g/mL}$

ethidium bromide in 1 X TAE buffer for 15 minutes and visualized using the Eagle Eye II Stratagene system (Preparation of Transforming DNA).

Sequencing of Mutants in pPICZ α A

To ensure that the ligation into the PICZ plasmid was successful, the sequence of the gene insert was determined for the H15S and the H15S+N77H mutants in pPICZ α A. The solutions for sequencing were prepared based on the protocol described in the instructions of the DTCS Sequencing Kit (*Beckmann Coulter*): 5 μ L of 40 ng/ μ L H15S or H15S+N77H DNA, 2 μ L of 10 μ M 3'AOXI (5'GCAAATGGATTCTGACATCC 3') or 5'AOXI (5'GACTGGTTCCAATTGACAAGC3') primer, and 8 μ L of DTCS Master Mix. The volume brought was up to 20 μ L using sterile water. The reagents were added in the following order: water, DNA, primers, DCTS Master Mix. The PCR program was as follows: an initial heat denaturation at 96 °C for 2 minutes, then a loop repeated 30 times consisting of heat denaturation at 96 °C for 20 seconds, annealing at 50 °C for 20 seconds, and extension at 60 °C for 4 minutes. The rest of the protocol was as earlier described (*GenomeLab DTCS with Quick Start Kit*, 2007).

Competent Cell Generation for Electroporation

The system chosen for protein expression was the yeast *Pichia pastoris*. *Pichia pastoris* is as easy to manipulate as other common simple eukaryotic organisms and it is less expensive and usually gives higher expression levels. *P. pastoris* is a methylotrophic yeast, meaning that it can metabolize methanol as a food source. The X-33 strain, or the wild-type strain, of *P. pastoris* was used (General Characteristics of *Pichia pastoris*).

The X-33 strain (*Invitrogen*) was streaked on a YPD (1.0% yeast extract, 2.0% peptone, 2.0% dextrose, 2.0% agar) plate and was incubated at 30 °C for at least 3 days.

One colony was chosen and inoculated into 10 mL of YPD broth and shaken overnight at 250 rpm at 30 °C. The cells were grown to an OD₆₀₀ of 1.3-1.5 absorbance units, which took about 16-18 hours. To make the cells competent, the following procedure was followed. The cells were harvested by centrifugation at 3,000 rpm at 4 °C for 5 minutes. The supernatant was decanted and the cells were re-suspended in 8 mL of a solution consisting of 100 mM LiCl, 10 mM DTT, 0.6 M sorbitol, and 10 mM Tris-HCl pH 7.5 and incubated at room temperature for 30 minutes (Wu & Letchworth, 2004). The cells were harvested by centrifugation at 3,000 rpm at 4 °C for 5 minutes. The supernatant was decanted and the cells were re-suspended in 500 mL of ice cold sterile water and the cells were centrifuged at 3,000 rpm at 4 °C for 5 minutes. The supernatant was decanted and the cells were re-suspended in 250 mL of ice cold sterile water. The cells were centrifuged at 3,000 rpm at 4 °C for 5 minutes and the supernatant was decanted. The cells were re-suspended in 20 mL of ice cold 1.0 M sorbitol and centrifuged at 3,000 rpm at 4 °C for 5 minutes. The supernatant was decanted and the cells were re-suspended in 1 mL of ice cold 1.0 M sorbitol. The competent cells were then used immediately for transformation by electroporation (Preparation of Pichia for Electroporation).

Transformation of Yeast by Mutant HEWL in pPICZ α A by Electroporation

A volume of 80 μ L of X-33 competent cells were mixed with 10 μ L of linearized DNA (H15S, H15S+N77H, or pPICZ α A) and were transferred to an ice cold 2 mm electroporation cuvette and incubated on ice for 5 minutes. The cells were then pulsed at 1.5 kV, 25 μ F, and 186 Ω . Then the cells were immediately washed with ice cold 1.0 M sorbitol and the contents were transferred to a 15 mL sterile tube. The tube was then incubated for 1.5 hours at 30 °C. Differing volumes between 10-200 μ L were spread on

YPDS plates (0.5% yeast extract, 1.0% peptone, 2.0% dextrose, 1.0 M sorbitol, 2.0% agar) containing 100 µg/mL Zeocin. The plates were incubated at 30 °C for at least 3 days. Any colonies that grew were re-streaked on YPD plates with 100 µg/mL Zeocin and incubated for at least 3 days at 30 °C.

Determining the Mut Phenotype

To determine the phenotype of the colony (Mut⁺ or Mut^S), each colony was spotted on both MDH (1.34% yeast nitrogen base, 4x10⁻⁵% biotin, 2% dextrose, 1.5% agar) and MMH (1.34% yeast nitrogen base, 4x10⁻⁵% biotin, 2% methanol, 1.5% agar) plates. If the rate of the growth of the colony is nearly the same on both plates, then the colony has a Mut⁺ phenotype. If the colony only grows on the MDH medium and not on the MMH medium, then the colony has a Mut^S phenotype. A set of replica plates was also prepared and replicates of the spotting were made using sterile felt. Both of the mutants, the plasmid pPICZα A, and a control GS115/lacZ/Mut⁺ were spotted. The plates were incubated at 30 °C for 2 days (Determining the Mut Phenotype).

Confirmation of Yeast Transformation by Polymerase Chain Reaction

To confirm that the mutant DNA in the pPICZα A plasmid was inserted into the genome of the X-33 strain of *Pichia pastoris*, the DNA was isolated and PCR was performed. The isolation procedure of DNA from *Pichia pastoris* was adopted from Harju, et al (Harju, Fedosyuk, & Peterson, 2004). A fresh 1.5 mL liquid culture of yeast was grown overnight at 30 °C in YPD plus 100 µg/mL Zeocin shaking at 225 rpm. The cells were harvested by centrifugation at 13,000 rpm for 3 minutes and the supernatant was removed. A volume of 200 µL of Harju buffer was added to the cells (2% Triton X-100, 1% SDS, 100 mM NaCl, 10 mM Tris-HCl pH 8.0, and 1 mM EDTA). The tubes

were then immersed in a dry ice/ethanol bath for 2 minutes. Then the tubes were immediately transferred to a heat block set at 95 °C for 1 minute. This freeze/thaw cycle was repeated 2 more times. The tubes were then vortexed for 30 seconds. 200 µL of chloroform were added and the tubes were vortexed for 2 minutes. The tubes were then centrifuged at 13,000 rpm for 3 minutes at room temperature. The upper aqueous layer was transferred to a new tube that contained 400 µL of ice cold 100% ethanol. The tube was mixed by inversion. The tube was incubated for 5 minutes at room temperature and then incubated for 10 minutes at -20°C. The tube was centrifuged for 5 minutes at room temperature at 13,000 rpm and the supernatant was removed. The pellet was washed with 500 µL of room temperature 70% ethanol and again centrifuged at 13,000 rpm for 5 minutes. The supernatant was removed and the pellet was dried using a CentriVap DNA Concentrator (*LABCONCO*) at 37 °C for 15 minutes. The pellet was re-suspended in 30 µL of 1X TE buffer. An RNase treatment was performed to remove unwanted RNA by adding 1 µL of 10 µg/mL RNase, and the tube was incubated at 37 °C for 30 minutes. Then 1/10th volume of 3 M NaCH₃COO pH 6.8 and 2 times the volume of 95% ethanol were added and the sample was incubated on ice for 10 minutes. The tube was centrifuged at 13,000 rpm for 5 minutes at room temperature and the supernatant was removed. The pellet was washed with 10 µL of room temperature 70% ethanol and was dried using a CentriVap DNA Concentrator (*LABCONCO*) at 37 °C for 30 minutes. The DNA was dissolved in 30 µL of 1X TE buffer (Eliminating the RNA from your DNA).

For the H15S+N77H mutant, the protocol for the PCR was as follows: 5 µL of 2 ng/µL H15S+N77H DNA, 1 µL of 10 mM dNTPs, 2 µL of 10 µM 3' AOXI, 2 µL of 10 µM 5' AOXI, and 10 µL of Promega Master Mix. The PCR reaction was performed with

a thermocycler (Techgene version 10.19) and the program was as follows: an initial heat denaturation at 94 °C for 2 minutes, then a loop repeated 30 times consisting of heat denaturation at 94 °C for 1 minute, annealing at 52 °C for 1 minute, and extension at 72 °C for 1 minute. The program ended with a final extension at 72 °C for 10 minutes. The reaction was loaded on a 1% agarose gel and was run at 85 V for 50-55 minutes. The gel was soaked in a solution of 5 µg/mL ethidium bromide in 1 X TAE buffer for 15 minutes and visualized using the Eagle Eye II Stratagene system.

2.3: Expression of Mutant Proteins

Small-Scale Expression

Several different conditions were tested to see which media would give the highest expression of lysozyme. Growth of *P. pastoris* occurs in two phases. The first growth is a general growing phase in YPD media. The broth of the second growth lacks glucose so that the yeast is forced to metabolize methanol. This promotes the expression of any gene located after the alcohol oxidase promoter. Two different conditions were used for the first growth: YPD without Zeocin and YPD with 100 µg/mL Zeocin. A colony was inoculated into 3 mL of each broth and each was incubated at 30 °C with shaking at 225 rpm for 24 hours. For the second growth, four different media were used: YPM/0.5 (1% yeast extract, 2% peptone, 0.5% methanol), YPM/2 (1% yeast extract, 2% peptone, 2.0% methanol), BMM/6 (100 mM phosphate buffer pH 6.2, 4x10⁻⁵% biotin, 1.34% yeast nitrogen base, 0.5% methanol), and BMM/7 (100 mM phosphate buffer pH 7.5, 4x10⁻⁵% biotin, 1.34% yeast nitrogen base, 0.5% methanol). The cells from the first growth were pelleted by centrifugation at 13,000 rpm for 3 minutes. The cells were then re-suspended in 3 mL of one of the previous 4 media and incubated for 5 days at 30 °C

with shaking at 225 rpm. A 500 μ L aliquot was taken every 24 hours. Every 24 hours the cells were also induced by adding 100% methanol to the growth media to a final concentration of 0.5% methanol (Liu, Saito, Azakami, & Kato, 2003).

2.4: Analysis of Mutant Proteins

Turbidimetric Assay

Lysozyme activity was monitored in the supernatant using a turbidimetric assay. A set of lysozyme standards was prepared in sterile water with the following concentrations of lysozyme: 0.004 mg/mL, 0.005 mg/mL, 0.006 mg/mL, 0.007 mg/mL, and 0.008 mg/mL. A solution of 0.3 mg/mL *Micrococcus lysodeikticus* (Sigma Aldrich) in 0.1 M phosphate buffer pH 7.0 was also prepared. The reaction was performed at 25°C and the lysozyme standards were kept on ice. A volume of 2.9 mL of the *M. lysodeikticus* cells were placed in a 1 cm cuvette and allowed to equilibrate to 25°C for at least 5 minutes. Then 100 μ L of one of the lysozyme standards was added and the absorbance at 450 nm was monitored for 150 seconds. A rate between 0.015-0.04 $\Delta A_{450}/\text{min}$ was optimal (Morsky, 1983). A total of 80 samples (both H15S+N77H and H15S with all eight different medium at each of the five 24-hour marks) were assayed using this procedure.

SDS-PAGE

Pre-cast gels were purchased from *BIO-RAD* with a 12% resolving gel. A volume of 20 μ L of each sample was added to a volume of 20 μ L of 2X Protein Loading Dye (*AMRESCO*). The samples were heated at 95 °C for 3 minutes. Then the samples were centrifuged at 13,000 rpm for 30 seconds. A volume of 30 μ L was loaded into each well. The Wide Range Protein Molecular Weight Marker (*AMRESCO*) was also treated in the

above manner. The gel was run at 120 volts for about 1.5 hours, or until the tracking dye reached the bottom of the gel. The gel was removed and placed in a Tupperware container. To pre-stain the gel, the container was filled with 100 mL of DDI water and was put in the microwave for 1 minute. The water was removed and the process was repeated two more times. To stain the gel, 100 mL of Blue BANDit™ Protein Stain (*AMRESCO*) was added and put in the microwave for 1 minute. Then the gel was shaken for 15 minutes at 75 rpm. To de-stain the gel, the dye was decanted and the Tupperware was filled with 100 mL of DDI water and shaken for 30 minutes at 75 rpm (KimWipes were also placed in the Tupperware to soak up the extra dye). The water was removed and fresh water (and KimWipes) were placed in the container and it was allowed to de-stain overnight.

Chapter 3: Results

3.1: Generation of Site-Directed Mutants

Isolation of the Native Lysozyme Gene from hewl-pCR®4-TOPO®

The native gene for lysozyme was digested out of the *hewl-pCR®4-TOPO®* plasmid to serve as the template to generate mutants using PCR. This was done using two restriction enzymes, *XbaI* and *EcoRI*. An image of a 1% agarose gel with the results of the digestion is pictured in Figure 3.1. The band at 400 bp corresponds to the size of the native gene. The band was cut out of the gel and the DNA was extracted.

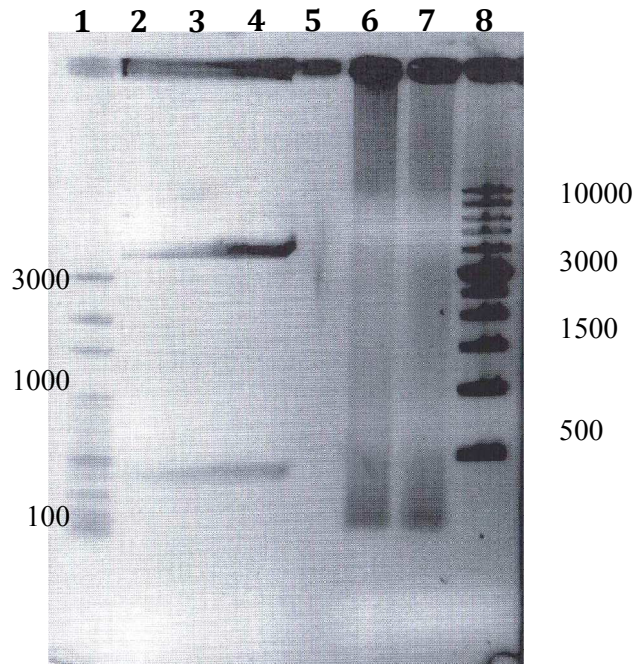


Figure 3.1: A gel image of the digestion of *hewl-pCR®4-TOPO®* using *XhoI* and *EcoRI*. Lane 1: 100 bp ladder; Lane 2-4: digestion of *hewl-pCR®4-TOPO®* containing the *hewl* gene; Lane 8: 1 kbp ladder.

Introducing the N103H Point Mutation

Primers N103HF and N103HR were employed, using the native *hewl* gene as template, to introduce a *hewl*-N103H mutation by the PCR overlap extension method.

Figure 3.2 shows an image of the results of the optimization of PCR amplification of the 5' and 3' fragments of the *hewl*-N103H mutation. The 5' fragment was about 300 bp in

size and the 3' fragment was approximately 100 bp in size, which corresponds to the position of the mutation within the sequence of the gene. The bands were cut out of the gel and the fragments were extracted.

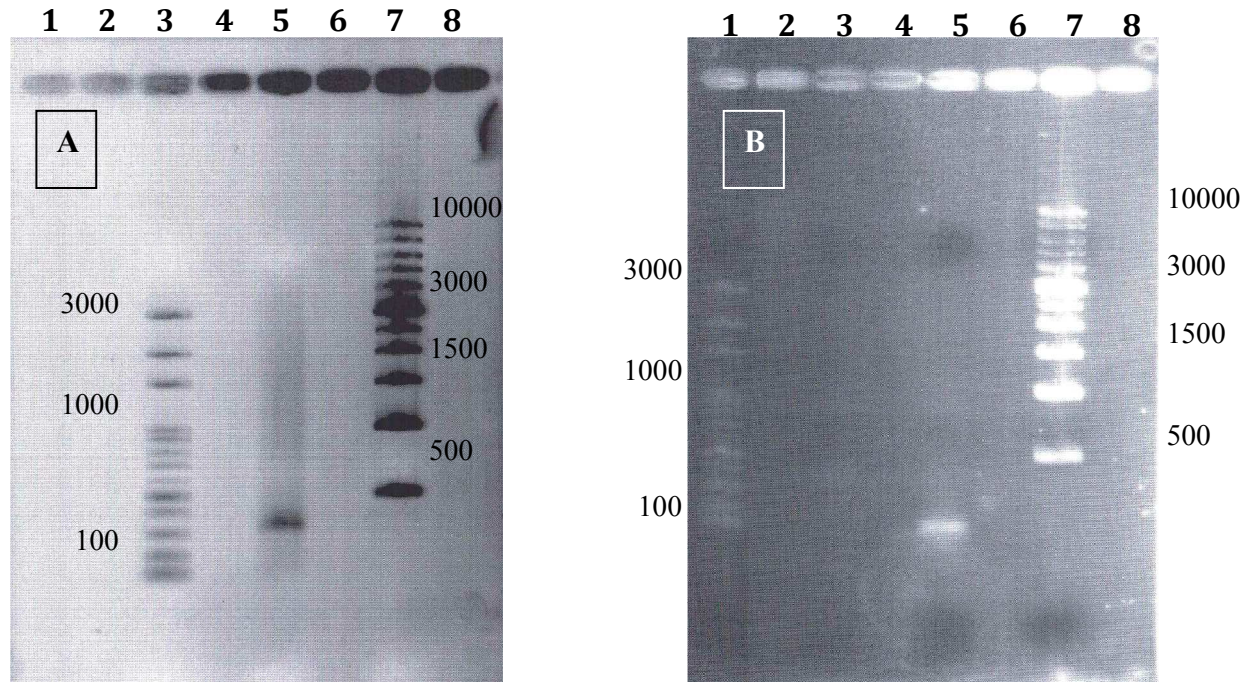


Figure 3.2: (A) A gel image of the 5' fragment end of mutant *hewl*-N103H using PCR. Lane 3: 100 bp ladder; Lane 5: 5' fragment end reaction; Lane 7: 1 kbp ladder. (B) A gel image of the 3' fragment end of mutant *hewl*-N103H using PCR. Lane 1: 100 bp ladder; Lane 5: 3' fragment end reaction; Lane 7: 1 kbp ladder.

Introducing the N77H Point Mutation

The same method was applied for the *hewl*-N77H mutation using the primers N2HF and N2HR. Figure 3.3 shows the results of the optimization of the PCR amplification of the 5' and 3' fragments of the *hewl*-N77H mutation. Both fragments were 200 bp in size, which corresponds to the position of the mutation within the gene sequence. The bands were cut out of the gel and the fragments were extracted.

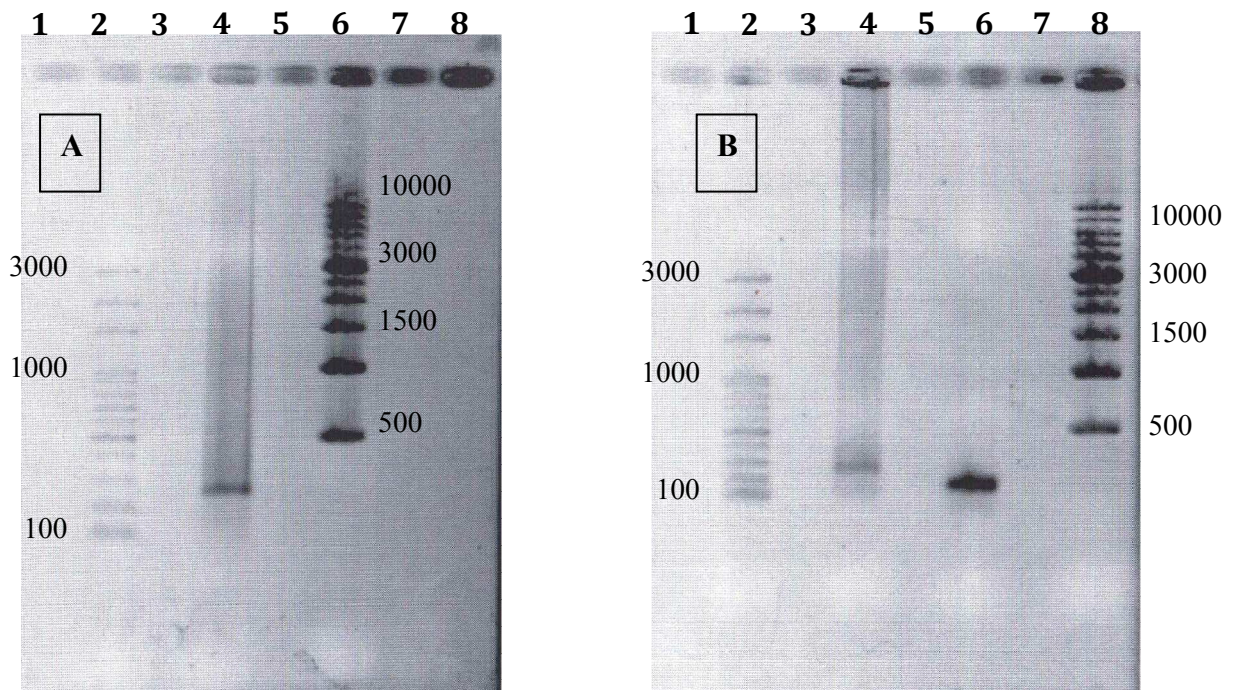


Figure 3.3: (A) A gel image of the 5' fragment end of mutant *hewl-N77H* using PCR. Lane 2: 100 bp ladder; Lane 4: 5' fragment end reaction; Lane 6: 1 kbp ladder. (B) A gel image of the 3' fragment end of mutant *hewl-N77H* using PCR. Lane 2: 100 bp ladder; Lane 4: 5' fragment end reaction; Lane 6: 3' fragment end reaction; Lane 8: 1 kbp ladder.

Splicing the 5' and 3' Fragments of the N103H and N77H Mutations

PCR conditions were optimized to generate the mutant fragments and each fragment was extracted from the agarose gel. The 5' and 3' fragments were then spliced together using PCR. The results of the splicing are shown in Figure 3.4. A band corresponding to the size of the gene (400 bp) was cut out of the gel and the DNA was extracted. The mutant genes were then cloned into pCR®4-TOPO® and the recombinant DNA was used to transform Mach1™ chemically competent *E. coli* cells, which were grown on LB media that contained ampicillin.

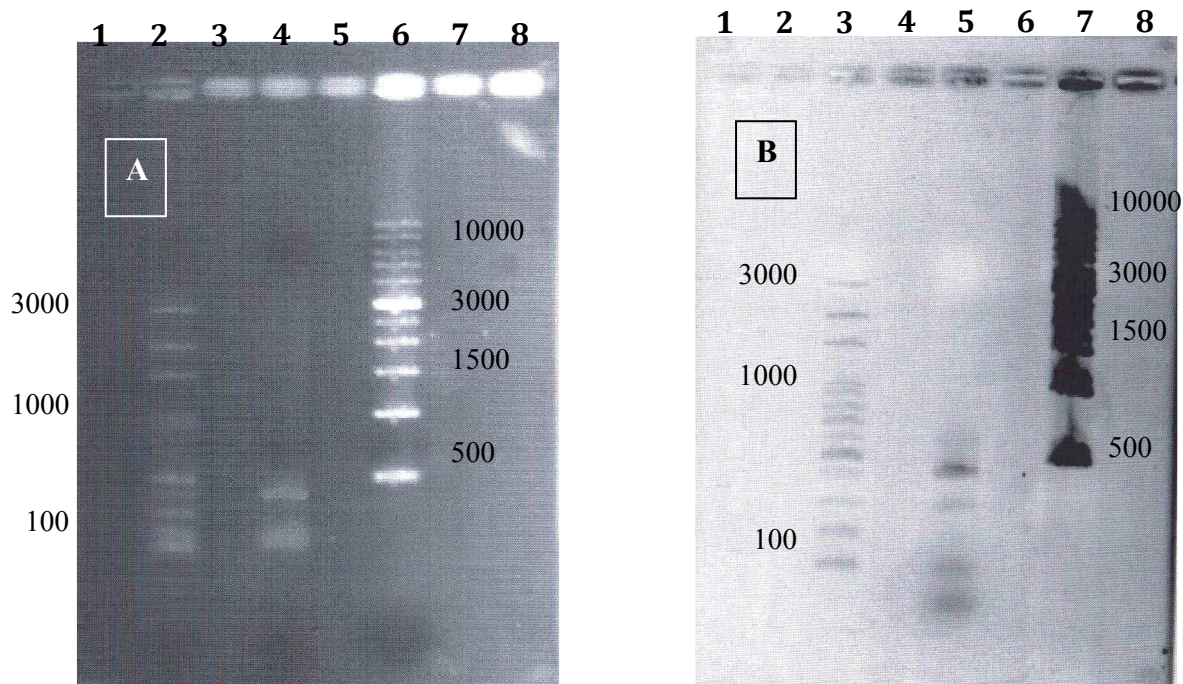


Figure 3.4: (A) A gel image of the splicing reaction of the 5' fragment and 3' fragment ends of the *hewl*-N103H mutation. Lane 2: 100 bp ladder; lane 4: splicing reaction; Lane 6: 1 kbp ladder. (B) A gel image of the splicing reaction of the 5' fragment and 3' fragment ends of the *hewl*-N77H mutation. Lane 3: 100 bp ladder; Lane 5: splicing reaction; Lane 7: 1 kbp ladder.

Confirmation of the Insertion of the hewl-N103H-TOPO® and hewl-N77H-TOPO®

After the mutant DNA was cloned into *pCR®4-TOPO®* and transformed into Mach1™ *E. coli* cells, the cells were grown overnight and the plasmid DNA was isolated. The DNA was then digested using 2 restriction enzymes to determine if the insertion of the mutant genes into *pCR®4-TOPO®* was successful. The restriction sites of *XhoI* and *XbaI* are positioned at the ends of the insert; therefore, when both of them are used, they should cut out the insert/gene. The gel in Figure 3.5 shows 2 bands, one corresponding to the plasmid at 4 kbp and one corresponding to the mutant gene at 400 bp.

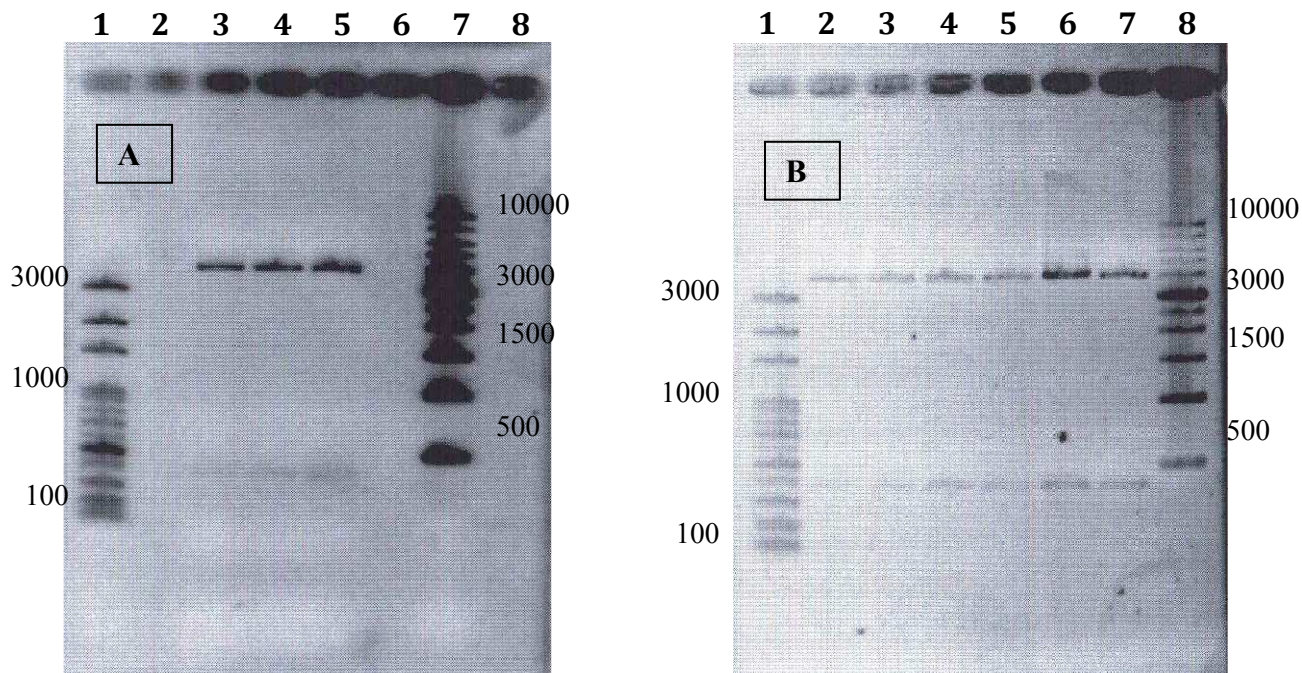
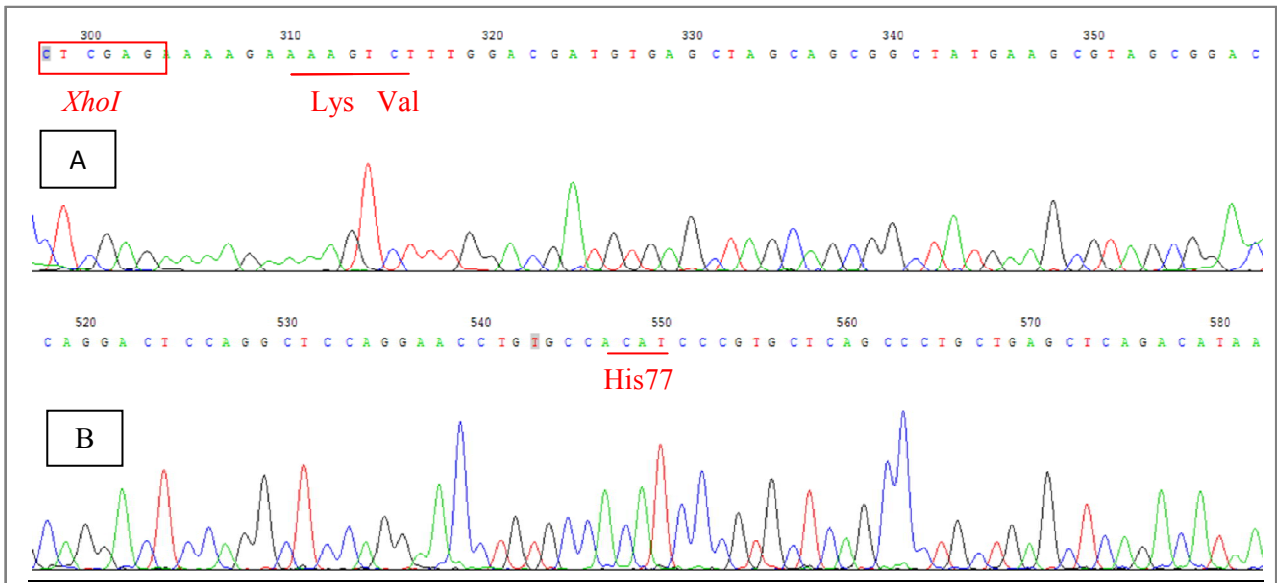


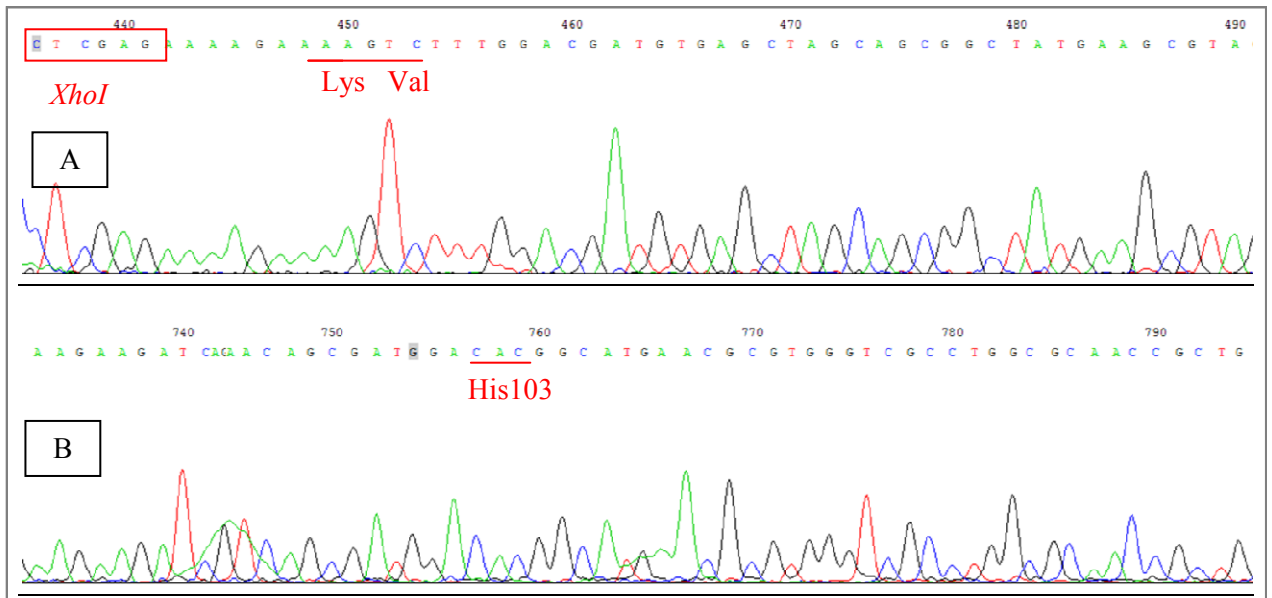
Figure 3.5: (A): A gel image of the double digest of the *hewl*-N103H-TOPO® mutant using *XhoI* and *XbaI*. Lane 1: 100 bp ladder; Lane 3-5: double digest reaction of plasmid isolated from 3 different transformed colonies; Lane 7: 1 kbp ladder. (B): A gel image of the double digest of the *hewl*-N77H-TOPO® mutant using *XhoI* and *XbaI*. Lane 1: 100 bp ladder; Lane 2-7: double digest reaction of plasmid isolated from 6 different transformed colonies; Lane 8: 1 kbp ladder.

Sequence of Mutant Genes in TOPO® Vector

After the presence of a gene of the right size was confirmed by a double digestion, the recombinant DNA was sequenced. Sequencing ensures that the mutation of the DNA base was in the correct position and yielded the desired codon change. Figures 3.6 and 3.7 show sections of the chromatogram where the mutation site was located and also the *XhoI* site.



ence of the *XhoI* restriction site (box)
(C) The sequence of the mutant



ence of the *XhoI* restriction
are shown. (C) The

3.2: Transformation into Competent Yeast

Preparation of Yeast Vector pPICZα A for Ligation

The plasmid chosen for protein expression in the yeast *Pichia pastoris* was pPICZα A. The plasmid was double digested with the restriction enzymes *XhoI* and *XbaI*

in preparation for cloning. Figure 3.8 shows the gel image after digestion. The gel shows one band corresponding to the size of the linearized plasmid at 3.6 kbp.

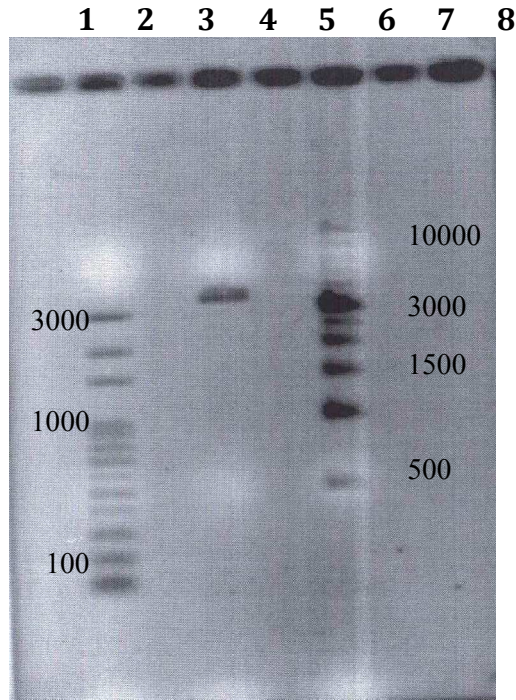


Figure 3.8: A gel image of the digestion of pPICZ α A for preparation for ligation. Lane 2: 100 bp ladder; Lane 4: digestion reaction; Lane 6: 1 kbp ladder.

Preparation of the Mutant Genes for Ligation into pPICZ α A

The mutant genes were digested out of the recombinant pCR $\text{\textcircled{R}}$ 4-TOPO $\text{\textcircled{R}}$ plasmid in preparation for cloning into the pPICZ α A plasmid. The double digestion of around 200 nanograms of *hewl*-N103H-TOPO $\text{\textcircled{R}}$ and *hewl*-N77H-TOPO $\text{\textcircled{R}}$ was performed using the restriction enzymes *Xho*I and *Xba*I. The bands at 400 bp were extracted from the agarose gel. Figure 3.9 show two gels displaying the 2 bands corresponding to the plasmid (4 kbp) and the *hewl*-N103H gene and *hewl*-N77H gene, respectively (400 bp).

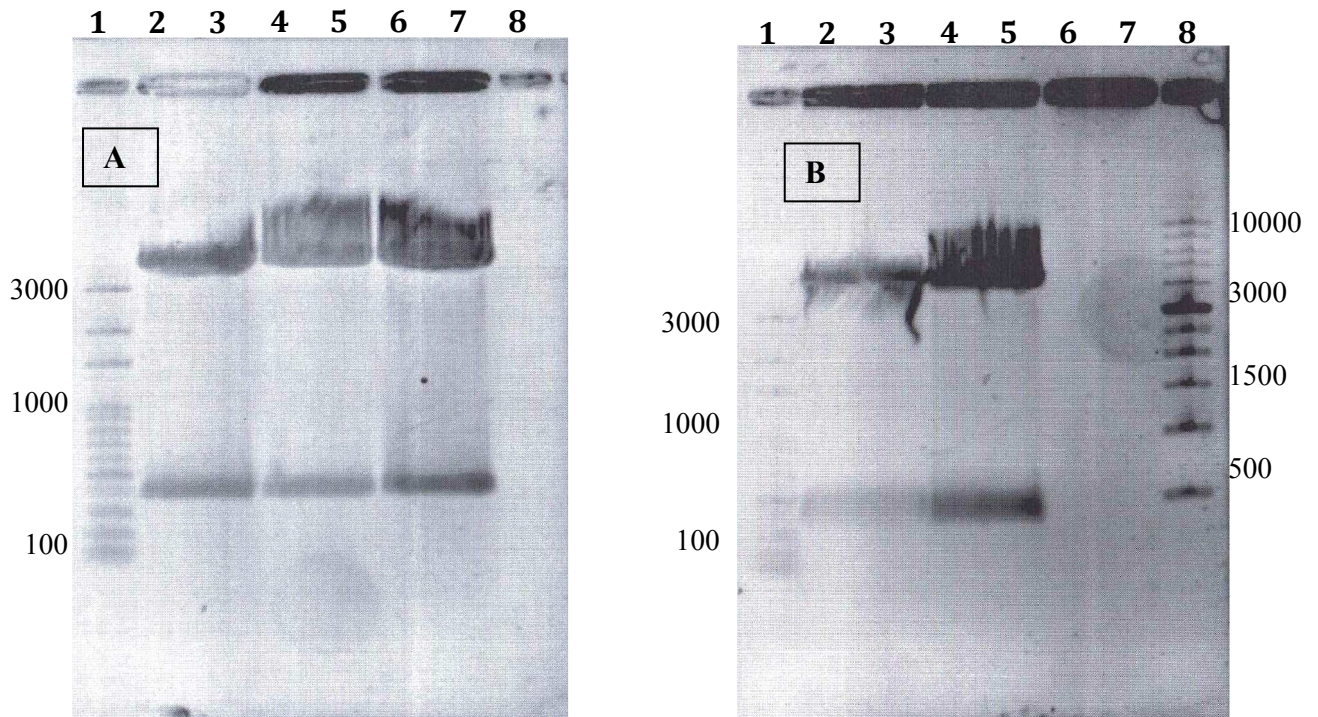


Figure 3.9: (A) A gel image of the double digest of *hewl*-N103H-TOPO® using *XhoI* and *XbaI*. Lane 1: 100 bp ladder; Lane 2&3, 4&5, 6&7: digestion reaction from 3 different transformed colonies. (B) A gel image of the double digest of *hewl*-N77H-TOPO® using *XhoI* and *XbaI*. Lane 1: 100 bp ladder; Lane 2&3, 4&5: digestion reaction from 2 different transformed colonies; Lane 8- 1 kbp ladder.

Ligation of the Mutant Genes into the pPICZα A Plasmid

The isolated mutant *hewl* genes and linearized pPICZα A plasmid were ligated using the Quick Ligation® Kit. After the ligation, the *hewl*-N103H-PICZα A and the *hewl*-N77H-PICZα A plasmids were then transformed into Mach1 chemically competent *E. coli* cells and grown on low salt LB medium plates containing 100 µg/mL Zeocin plates. The *hewl*-N103H gene was ligated successfully as seen by a full plate of colonies that are Zeocin resistant. However, the lack of any colonies indicated that the *hewl*-N77H mutant did not ligate successfully.

Sequence of Mutants in pPICZα A

To move forward on the project, the focus was then switched to the *hewl*-H15S-PICZα A and the *hewl*-H15S+N77H-PICZα A mutants. To ensure that the gene was

inserted properly into the pPICZ α A plasmid, its sequence was determined. Two sequencing reactions were prepared using either the 3' AOXI or 5' AOXI primer. Segments of each mutant sequence are shown in Figures 3.11 and 3.12. Besides ensuring that the point mutation was retained, the restriction enzyme sites *XhoI* and *XbaI* also had to be present. *XhoI* is at the 3' end of the α -factor signal sequence which generates the signal peptide necessary for extracellular expression. The stop codon is found within the *XbaI* restriction enzyme site. By checking each of these components, it was confirmed that the gene was inserted into the correct reading frame of the α -factor signal sequence for extracellular expression.

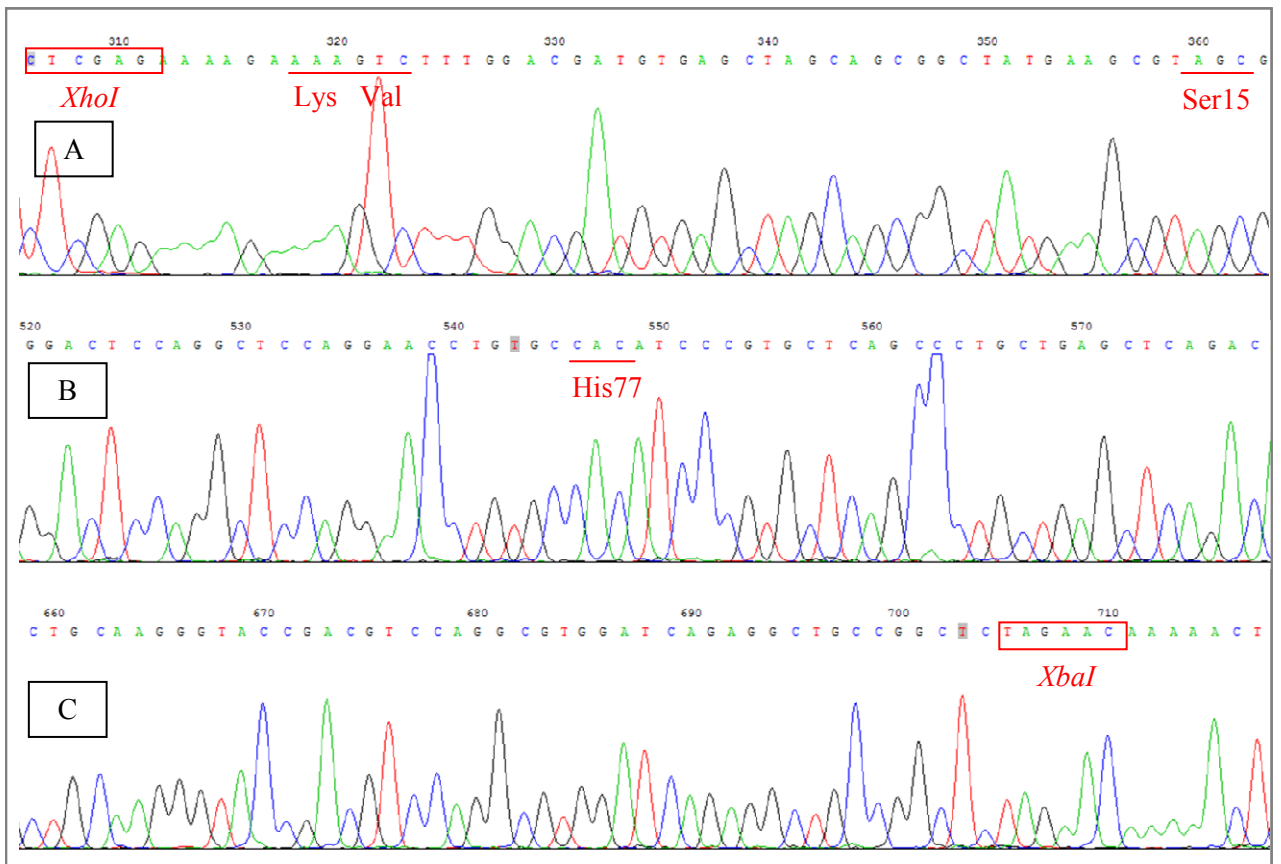
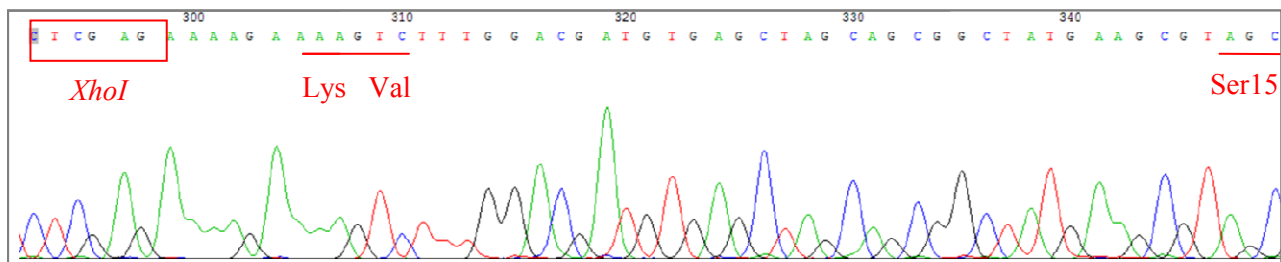


Figure 3.10: Sections of the chromatogram for the *hewl*-H15S+N77H-PICZ α A (A) The sequence of the *XhoI* restriction site (box) and the first 2 codons of the lysozyme gene (underline) are shown. One of the mutated codons, which codes for a serinyl residue, is also shown (underline). (B) The second mutated codon that codes for a histidyl residue is shown (underline) (C) The sequence for the *XbaI* restriction site (box) is shown for the lysozyme gene.



Location of the *XhoI* restriction site (box) and the start codon (underline), which codes for Ser15.

Linearization of Mutant *hewl* DNA for Yeast Transformation

The colonies of transformed Mach1 cells with *hewl*-H15S-PICZ α A and *hewl*-H15S+N77H-PICZ α A were grown overnight, and the DNA was isolated using the QIAGEN® Plasmid Midi Kit. To linearize the DNA, the restriction enzyme *BstXI* was used. The digest was run on an agarose gel and the image is shown in Figure 3.10A. One single band at 4 kbp indicates that the pPICZ α A plasmid containing the mutant gene was linearized. The DNA was then extracted and its concentration determined by running another agarose gel. One of the gels is shown in Figure 3.10B.

For use as a control, the plasmid without a mutant gene insert was also linearized for yeast transformation. A double digest using the enzymes *XhoI* and *XbaI* was performed. A gel image of that linearization is also shown in Figure 3.10 A and B. One single band at 3.6 kbp was observed.

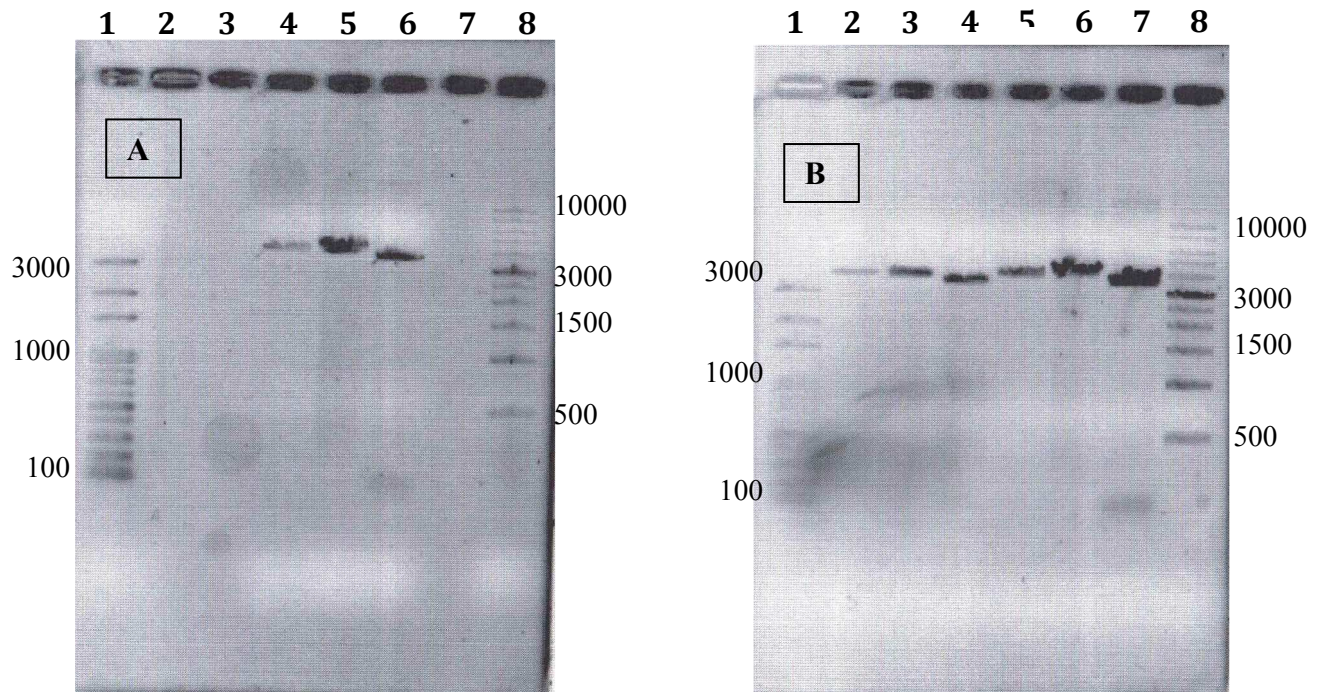


Figure 3.12: (A) A gel image of the linearization of *hewl*-H15S-PICZ α A, *hewl*-H15S+N77H-PICZ α A, and pPICZ α A with no insert, using *Bst*XI. Lane 1: 100 bp ladder; Lane 4: *hewl*-H15S+N77H-PICZ α A linearization; Lane 5: *hewl*-H15S-PICZ α A linearization; Lane 6: pPICZ α A linearization; Lane 8: 1 kbp ladder. (B) A gel image of the linearization of *hewl*-H15S-PICZ α A, *hewl*-H15S+N77H-PICZ α A, and pPICZ α A using *Bst*XI and determining the concentration of the previously linearized samples in (A). Lane 1: 100 bp ladder; Lane 2: concentration of linearized *hewl*-H15S+N77H-PICZ α A; Lane 3: concentration of linearized *hewl*-H15S-PICZ α A; Lane 4: concentration of linearized pPICZ α A; Lane 5: *hewl*-H15S+N77H-PICZ α A linearization; Lane 6: *hewl*-H15S-PICZ α A linearization; Lane 7: pPICZ α A linearization; Lane 8: 1 kbp ladder.

Generation of Competent Cells for Electroporation

After the X-33 *Pichia pastoris* cells were made competent for electroporation, a sample was streaked on YPD plates to ensure their viability. A picture of the resulting plate is shown in Figure 3.13B. Also in Figure 3.13A is a picture of the X-33 cells prior to being made competent.

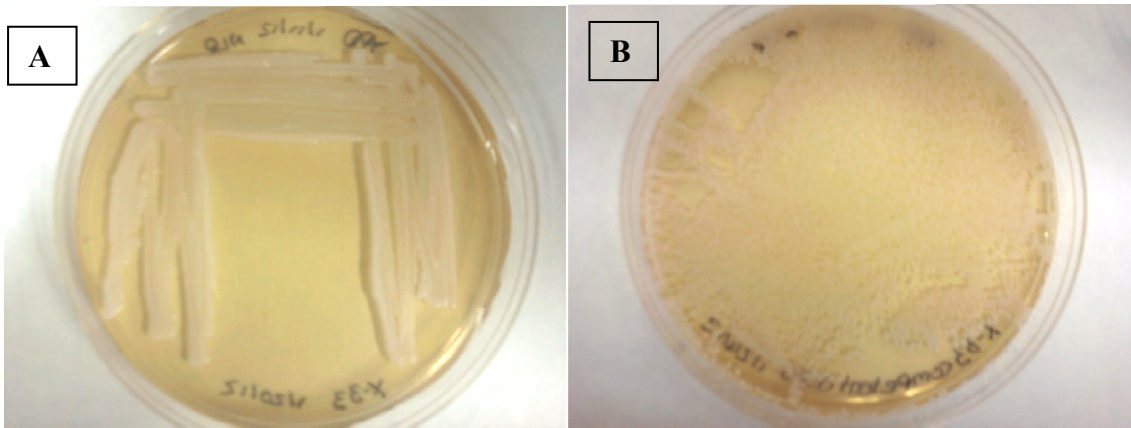
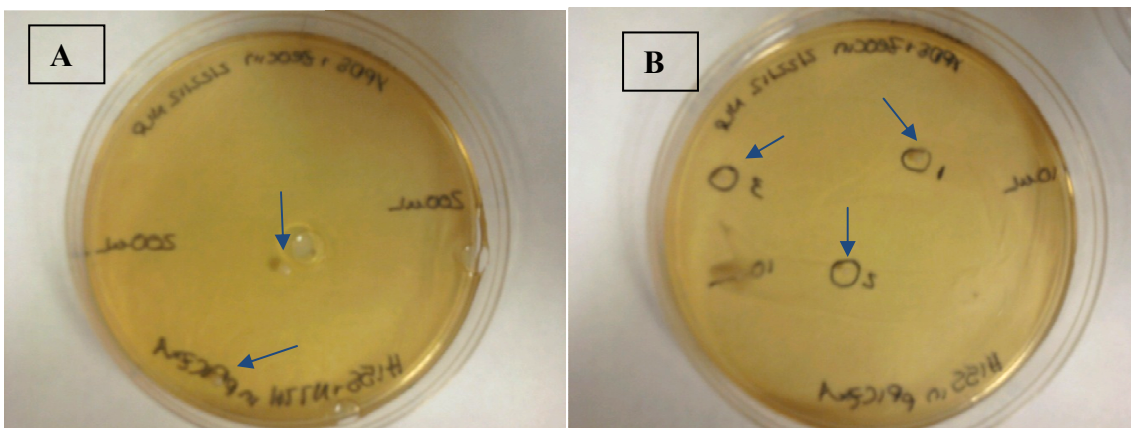


Figure 3.13: (A) A picture of the X-33 strain of *Pichia pastoris* before the cells were made competent. Yeast colonies are whiter in color and much larger than typical *E. coli* colonies. (B) A picture of the X-33 cells after they were made competent for electroporation. A sample of the competent cells was streaked to ensure their viability for transformation.

Mutant hewl Yeast Transformation by Electroporation

After the linearized recombinant DNA was transformed into *Pichia pastoris*, different volumes of the cells were grown on YPDS plates containing 100 $\mu\text{g}/\text{mL}$ Zeocin. A picture of those plates is shown in Figure 3.14A-D. To allow individual colonies to grow and to also ensure Zeocin resistance, selected colonies were re-streaked on YPD plates containing 100 $\mu\text{g}/\text{mL}$ Zeocin. A picture of some of those plates is shown in Figure 3.15A-C.



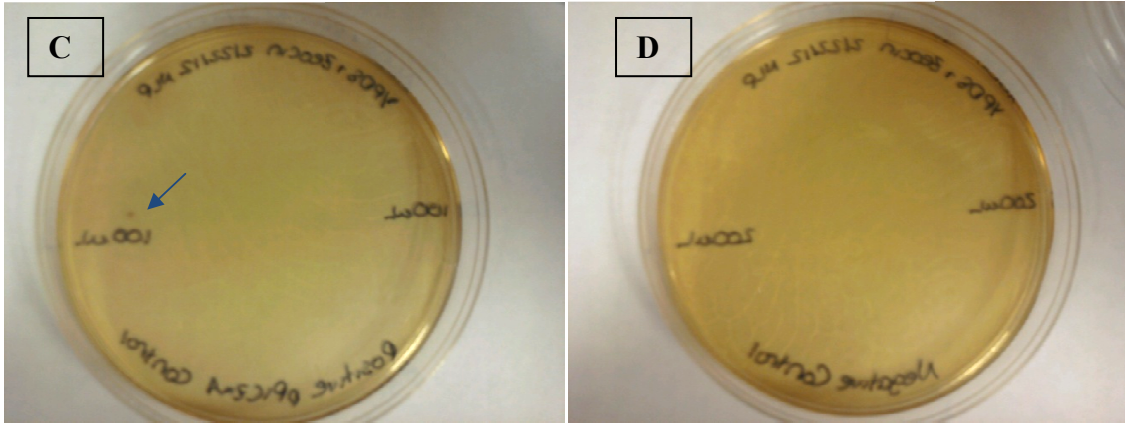


Figure 3.14: (A) A picture of the transformation of *hewl*-H15S+N77H-PICZ α A into competent yeast cells. A blue arrow points to 2 colonies that grew with a volume of 200 μ L plated. (B) A picture of the transformation of *hewl*-H15S-PICZ α A into competent yeast cells. A blue arrow points to 3 colonies that grew with a volume of 10 μ L plated. (C) A picture of the transformation of pPICZ α A into yeast competent cells. A blue arrow points to 1 colony that grew with a volume of 100 μ L plated. (D) A picture of the negative control, where no DNA was used for the transformation.

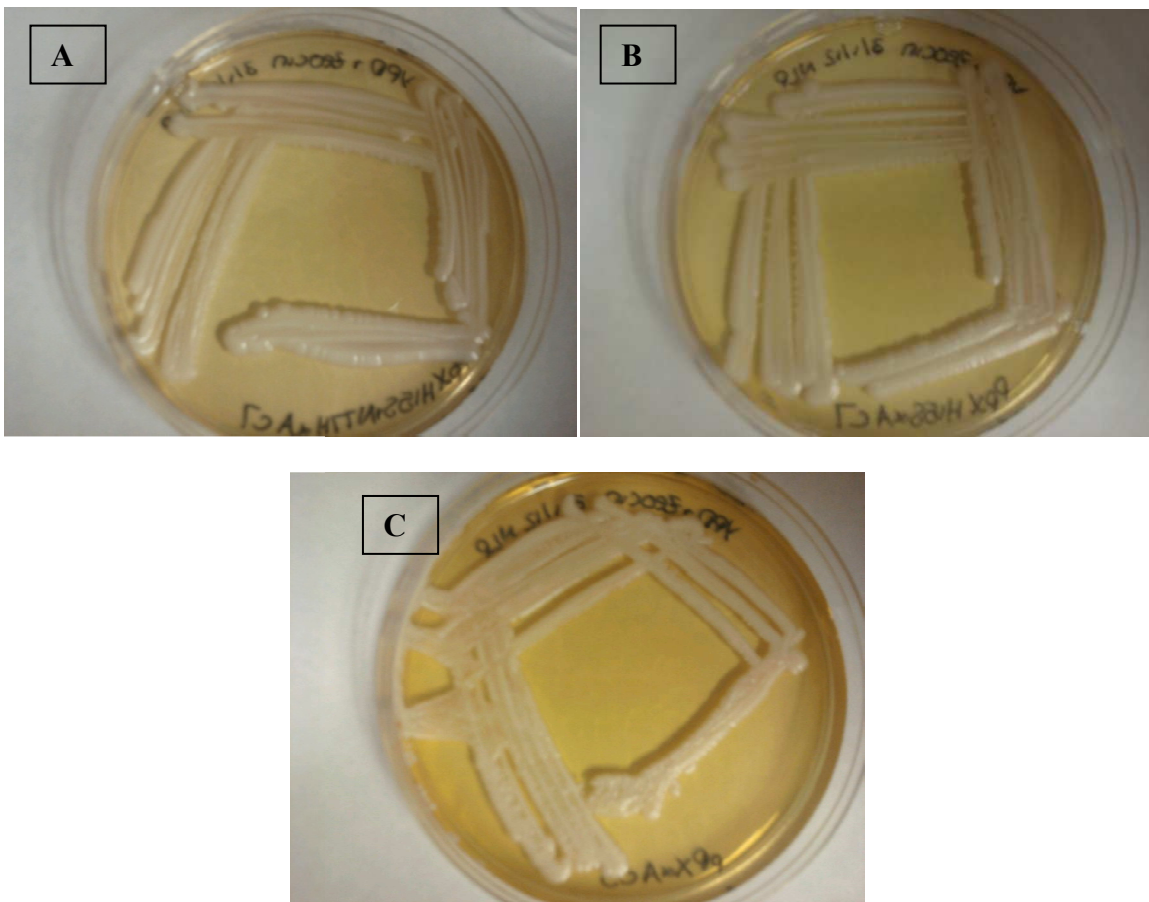


Figure 3.15: (A) A picture of the 7th colony of *hewl*-H15S+N77H-PICZ α A re-streaked. This colony was used for future small-scale expression experiments. (B) A picture of the 7th colony of *hewl*-H15S-PICZ α A re-streaked. This colony was used for future small-scale expression experiments. (C) A picture of the 3rd colony of pPICZ α A re-streaked. This colony was used for future small-scale expression experiments.

Determining the Mut Phenotype

To check the phenotype of the colonies, each colony was spotted on an MDH plate and an MMH plate. The phenotype of the X-33 strain should be Mut^+ because this yeast strain with pPICZ α A can metabolize methanol as a sole carbon source because of the presence of the alcohol oxidase gene. Therefore, the Mut^+ phenotype will grow at the same rate on both the MDH (dextrose) and MMH (methanol) plates. The pictures of the plates are shown in Figure 3.16. By seeing that all colonies grew on both plates, the phenotype of the colonies was confirmed as Mut^+ .

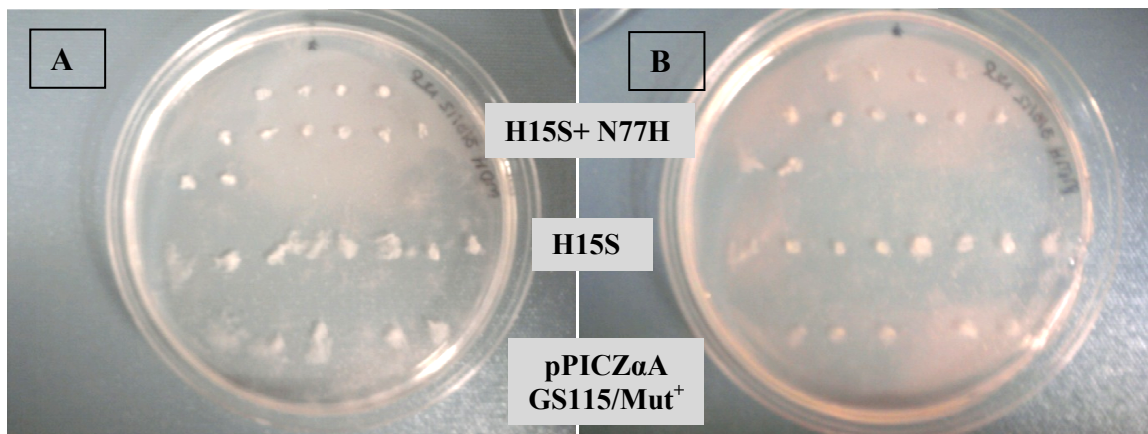


Figure 3.16: (A) A picture of the replication of each colony that grew for *hewl*-H15S+N77H-PICZ α A, *hewl*-H15S-PICZ α A, and pPICZ α A on an MDH plate. A GS115/ Mut^+ control was also replicated. (B) A picture of the replication of each colony that grew for *hewl*-H15S+N77H-PICZ α A, *hewl*-H15S-PICZ α A, and pPICZ α A on an MMH plate. A GS115/ Mut^+ control was also replicated. A Mut^+ phenotype grows at the same rate on both the glucose plate (MDH) and the methanol plate (MMH). The first 3 rows are colonies of *hewl*-H15S+N77H-PICZ α A, the fourth row is colonies of *hewl*-H15S-PICZ α A, and the last row are the controls, pPICZ α A and GS115/ Mut^+ .

PCR Analysis

To determine if the *hewl*-H15S-PICZ α A and *hewl*-H15S+N77H-PICZ α A DNA was integrated into the *Pichia pastoris* genome, the DNA was isolated and PCR was performed. The DNA was isolated using a protocol adapted from Harju et. al. and an RNase treatment was performed that was adapted from Cornell University's website. The PCR results of *hewl*-H15S+N77H-PICZ α A are shown in Figure 3.17. The primers

will typically amplify a 600 bp region of pPICZ α A, but with the addition of a 400 bp insert, a band at approximately 1000 bp verifies that the gene was integrated into the yeast genome.

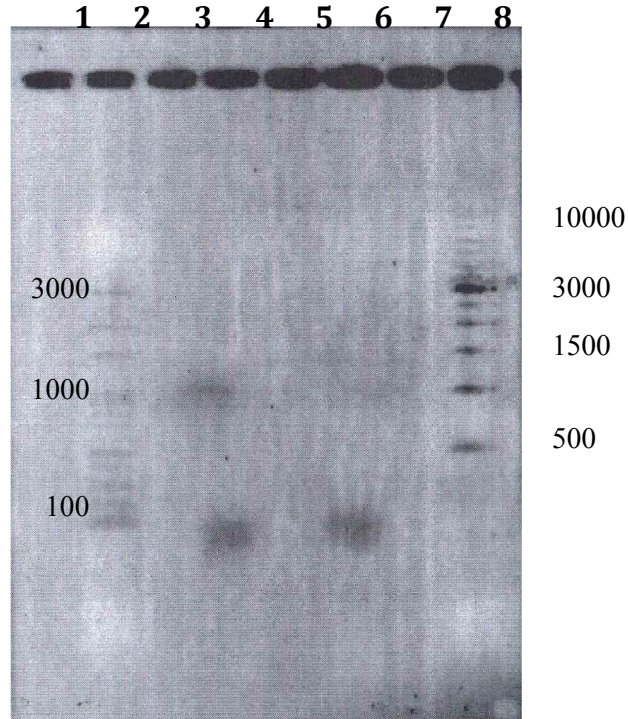


Figure 3.17: A gel image of the PCR results for *hewl*-H15S+N77H-PICZ α A. Lane 2: 100 bp ladder; Lane 4: PCR product *hewl*-H15S+N77H-PICZ α A; Lane 8: 1 kbp ladder. The bands that are below 100 bp are believed to be RNA still left in the sample.

3.3: Expression of Mutant Proteins

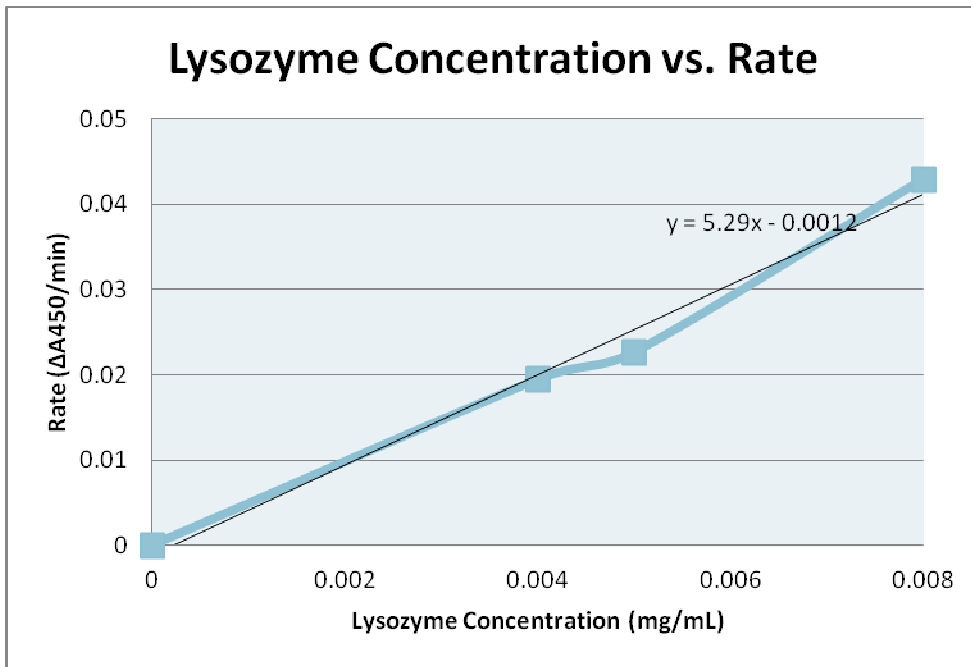
Small-Scale Expression

The optimal conditions for the extracellular expression of mutant lysozyme required an initial growth in YPD media with Zeocin for 24 hours at 30°C followed by the inoculation of YPM media (2% methanol) for 72-120 hours at 30°C. This conclusion was based on the analysis of mutant proteins by performing enzyme assays of samples at 24-hour increments and also SDS-PAGE analysis on the samples at 24-hour increments. The same conditions were applied to two control samples, pPICZ α A and the GS115/Mut⁺.

3.4: Analysis of Mutant Proteins

Turbidimetric Assay

The standards used for this assay had a concentration range of 0.004-0.008 mg/mL lysozyme. A standard curve is shown in Figure 3.18. The line fit to the standard curve was used to calculate an “Equivalent Concentration Unit” of the mutant proteins that retained lysozyme activity in the samples of growth media. Each of the time point samples for both HEWL-H15S+N77H and HEWL-H15S were assayed. Some graphs made from those results are shown in Figures 3.19-3.22.



cell lysis. The linear

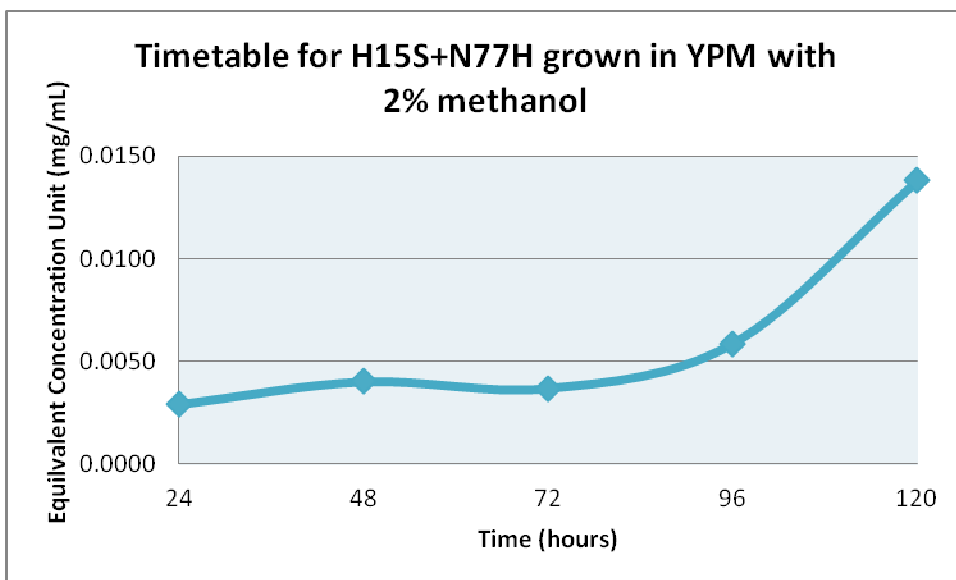


Figure 3.19: A graph showing the rate of HEWL-H15S+N77H mutant protein expression over a 120 hour period. This sample had a first growth in YPD with Zeocin and a second growth in YPM with 2% methanol.

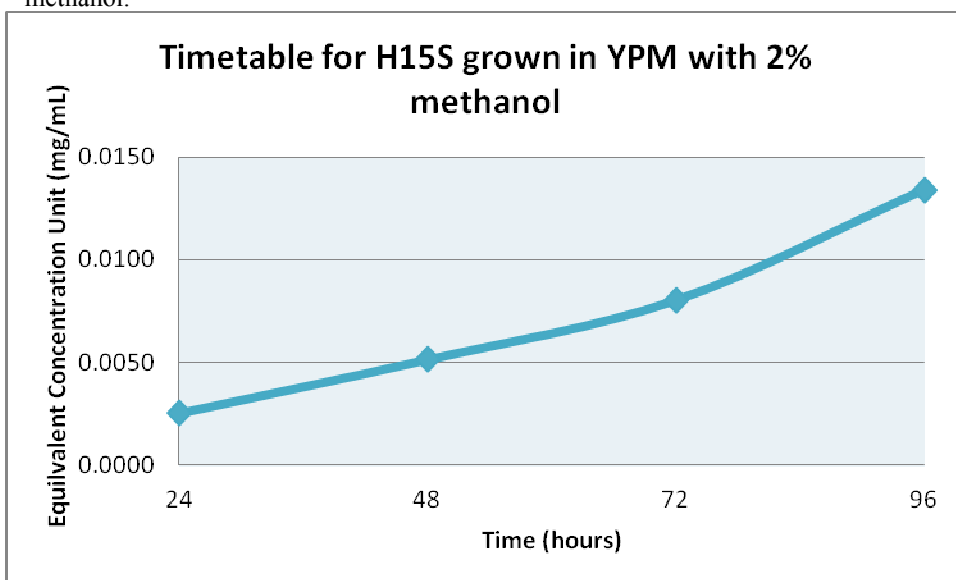


Figure 3.20: A graph showing the rate of HEWL-H15S mutant protein expression over a 96 hour period. This sample had a first growth in YPD with Zeocin and a second growth in YPM with 2% methanol.

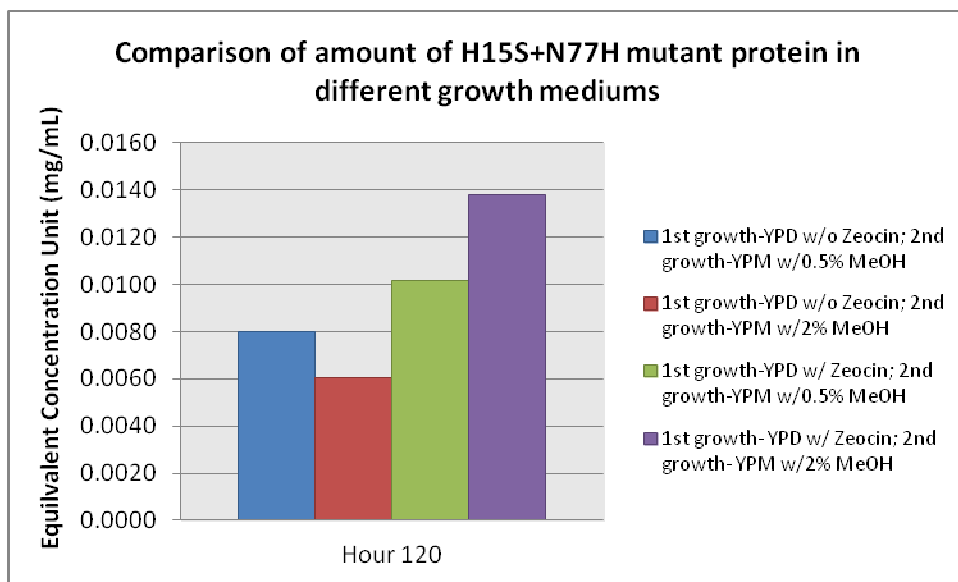


Figure 3.21: A graph showing the difference in amount of HEWL-H15S+N77H mutant protein at hour 120. This graph shows that the optimal expression conditions are a first growth in YPD with Zeocin and a second growth in YPM with 2% methanol.

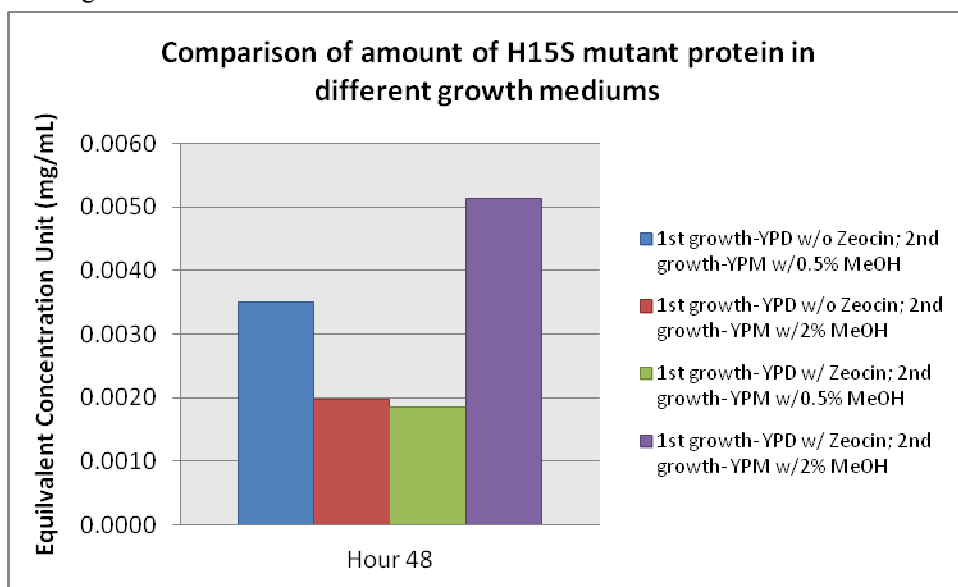


Figure 3.22: A graph showing the difference in amount of HEWL-H15S mutant protein at hour 48. This graph shows that the optimal expression conditions are a first growth in YPD with Zeocin and a second growth in YPM with 2% methanol. Hour 48 was the highest common time point among the *HEWL-H15S* samples; there was not enough sample in the other media to have greater time points.

As described in the Materials and Methods section, other conditions were also examined for optimal lysozyme expression. An overall comparison of each condition at each time point is shown in Figures 3.23 and 3.24.

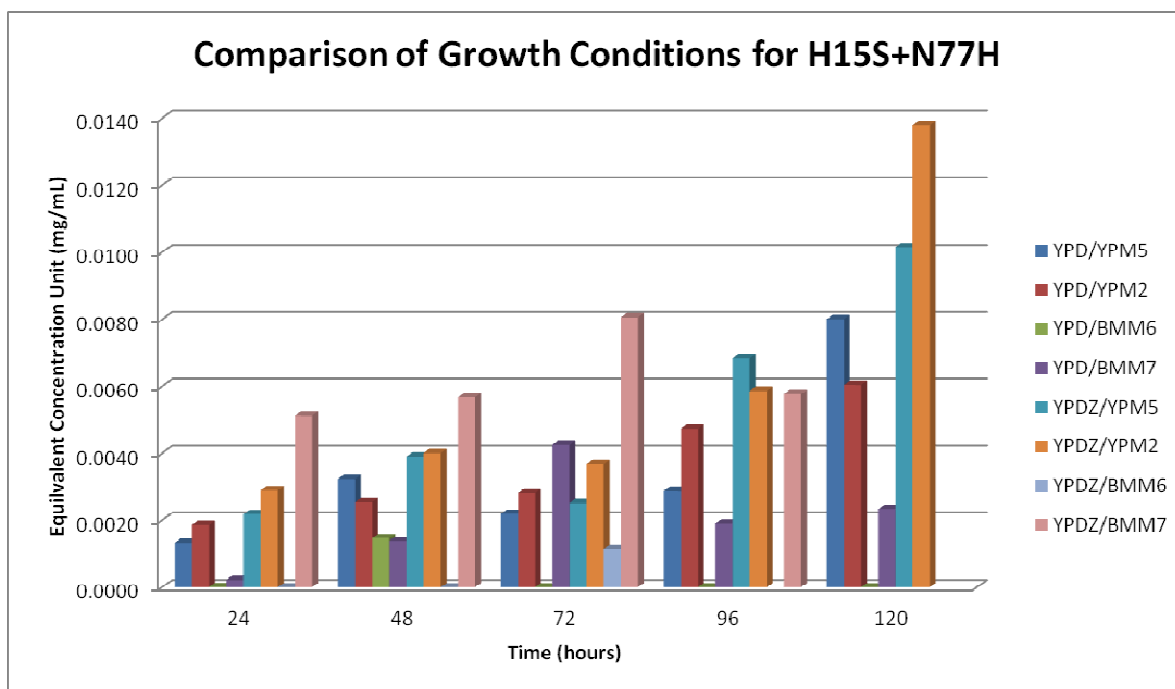


Figure 3.23: A graph showing the overall comparison of growth conditions and time points for the expression of HEWL-H15S+-N77H mutant protein. The key for the legend is as follows: YPD-YPD without Zeocin; YPDZ-YPD with Zeocin; YPM5-YPM with 0.5% initial methanol concentration; YPM2-YPM with 2.0% initial methanol concentration; BMM6-BMM with pH 6.2; BMM7-BMM with pH 7.5. This graph shows that D6 gives the best and most consistent overall expression of HEWL-H15S+-N77H mutant protein.

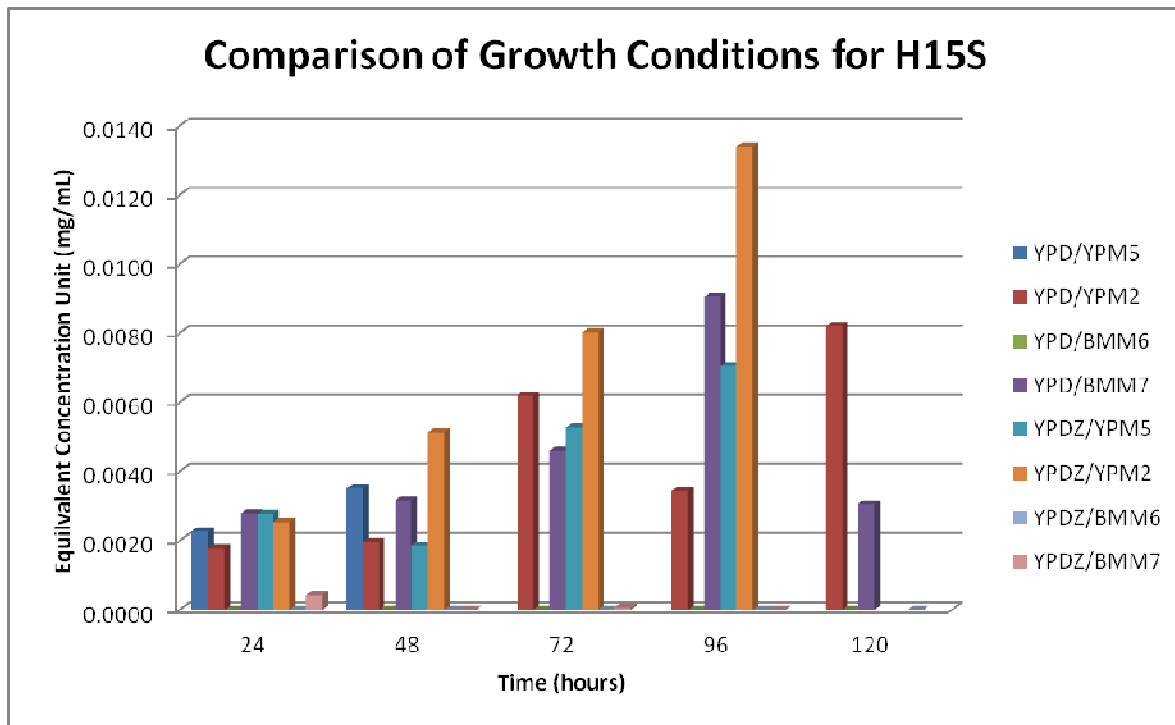


Figure 3.24: A graph showing the overall comparison of growth conditions and time points for the expression of HEWL-H15S mutant protein. The key for the legend is as follows: YPD-YPD without Zeocin; YPDZ-YPD with Zeocin; YPM5-YPM with 0.5% initial methanol concentration; YPM2-YPM with 2.0% initial methanol concentration; BMM6-BMM with pH 6.2; BMM7-BMM with pH 7.5. This graph shows that H6 gives the best and most consistent overall expression of HEWL-H15S mutant protein.

The controls, pPICZ α A and GS115/Mut⁺, were also grown under similar conditions and assayed. The results for the controls were inconsistent and nonlinear, indicating no protein with relative lysozyme activity was present in the samples. Figure 3.25 shows a comparison of the activity of the HEWL-H15S+N77H mutant protein in YPM media from 24-120 hours.

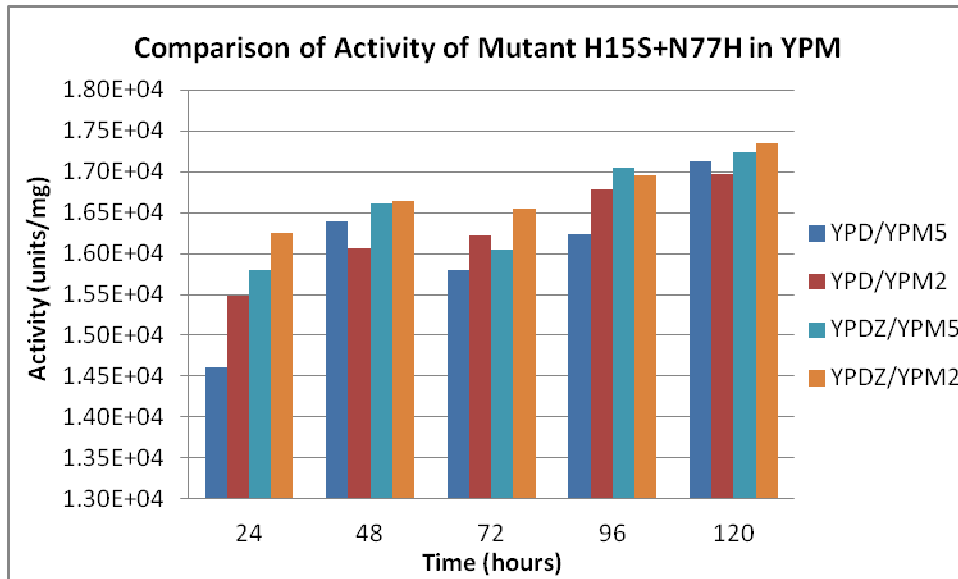


Figure 3.25: A graph showing the overall comparison of mutant HEWL-H15S+N77H protein activity between the YPM growth conditions. The key for the legend is as follows: YPD-YPD without Zeocin; YPDZ-YPD with Zeocin; YPM5-YPM with 0.5% initial methanol concentration; YPM2-YPM with 2.0% initial methanol concentration. This graph shows that the activity is relatively constant among the different growth conditions and that the activity increases slightly with increasing equivalent lysozyme concentration.

SDS-PAGE

To confirm the turbidimetric assays, SDS-PAGE was run to visualize the mutant proteins in the sample. Figure 3.26 shows the range of proteins in the four different conditions at the 72-hour time point for each mutant. Figure 3.27 shows the progression of the expression of protein in the same growth condition from 24-120 hours for both HEWL-H15S and HEWL-H15S+N77H.

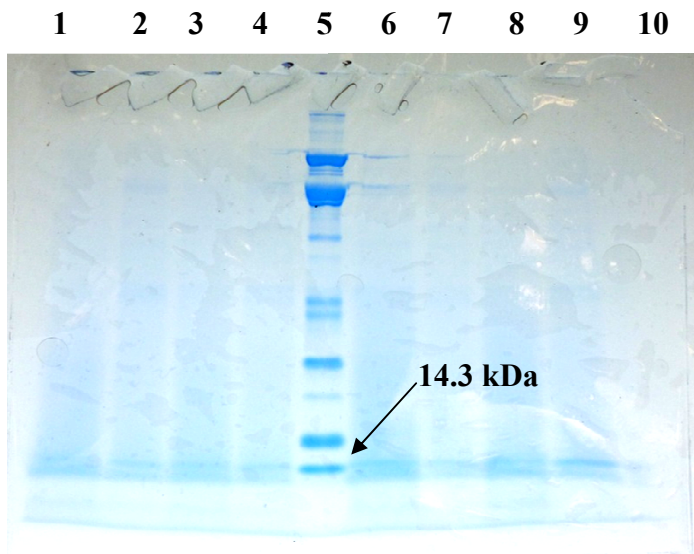


Figure 3.26: An SDS-PAGE of the YPM samples at hour 72. Lane 1: HEWL-H15S+N77H, YPD/YPM5; Lane 2: HEWL-H15S+N77H, YPD/YPM2; Lane 3: HEWL-H15S+N77H, YPDZ/YPM5; Lane 4: HEWL-H15S+N77H, YPDZ/YPM2; Lane 5: Protein marker; Lane 6: HEWL-H15S, YPD/YPM5; Lane 7: HEWL-H15S, YPD/YPM2; Lane 8: HEWL-H15S, YPDZ/YPM5; Lane 9: HEWL-H15S, YPDZ/YPM2. The key for the legend is as follows: YPD-YPD without Zeocin; YPDZ-YPD with Zeocin; YPM5-YPM with 0.5% initial methanol concentration; YPM2-YPM with 2.0% initial methanol concentration. Each sample shows a band at 14.3 kDa, which is the molecular weight of lysozyme. These samples also show 2 bands around the correct weight, which is a typical problem in the *Pichia pastoris* system.

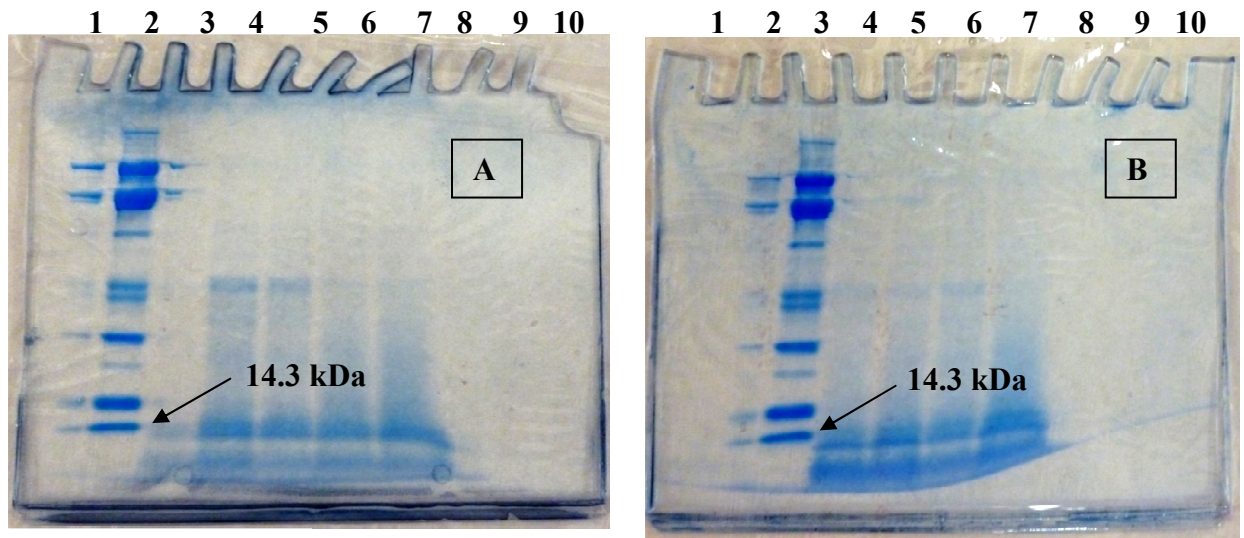


Figure 3.27: An SDS-PAGE of the time progression of the expression of mutant protein with the initial growth in YPDZ and the 5-day growth in YPM5. (A) The samples for HEWL-H15S+N77H mutant. Lane 2: protein marker; Lane 3: HEWL-H15S+N77H at hour 24; Lane 4: HEWL-H15S+N77H at hour 48; Lane 5: HEWL-H15S+N77H at hour 72; Lane 6: HEWL-H15S+N77H at hour 96; Lane 7: HEWL-H15S+N77H at hour 120. (B) The samples for HEWL-H15S mutant protein. Lane 3: protein marker; Lane 4: HEWL-H15S at hour 24; Lane 5: HEWL-H15S at hour 48; Lane 6: HEWL-H15S at hour 72; Lane 7: HEWL-H15S at hour 96.

An SDS-PAGE was run on the samples that were grown in BMM media as well.

The result is shown in Figure 3.28. The negative controls were also run on SDS-PAGE to check for the presence of lysozyme. That picture is shown in Figure 3.29.

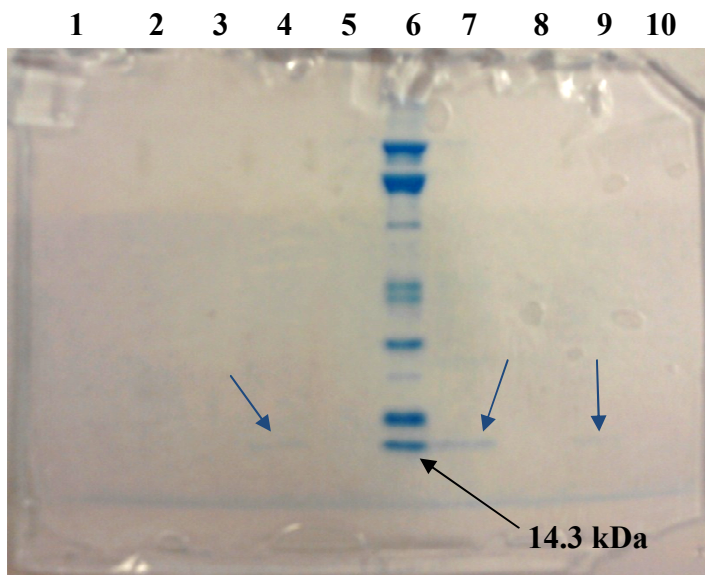


Figure 3.28: An SDS-PAGE of the samples grown in BMM medium at hour 72. Lane 2: HEWL-H15S+N77H in YPD/BMM6; Lane 3: HEWL-H15S+N77H in YPD/BMM7; Lane 4: HEWL-H15S+N77H in YPDZ/BMM6; Lane 5: HEWL-H15S+N77H in YPDZ/BMM7; Lane 6: Protein marker; Lane 7: HEWL-H15S in YPD/BMM6; Lane 8: HEWL-H15S in YPD/BMM7; Lane 9: HEWL-H15S in YPDZ/BMM6; Lane 10: HEWL-H15S in YPDZ/BMM7. The key for the legend is as follows: YPD-YPD without Zeocin; YPDZ-YPD with Zeocin; BMM6-BMM with pH 6.2; BMM7-BMM with pH 7.5. The samples in lanes 4, 7, and 9 show a band at 14.3 kDa as indicated by the blue arrows, which is the molecular weight of lysozyme.

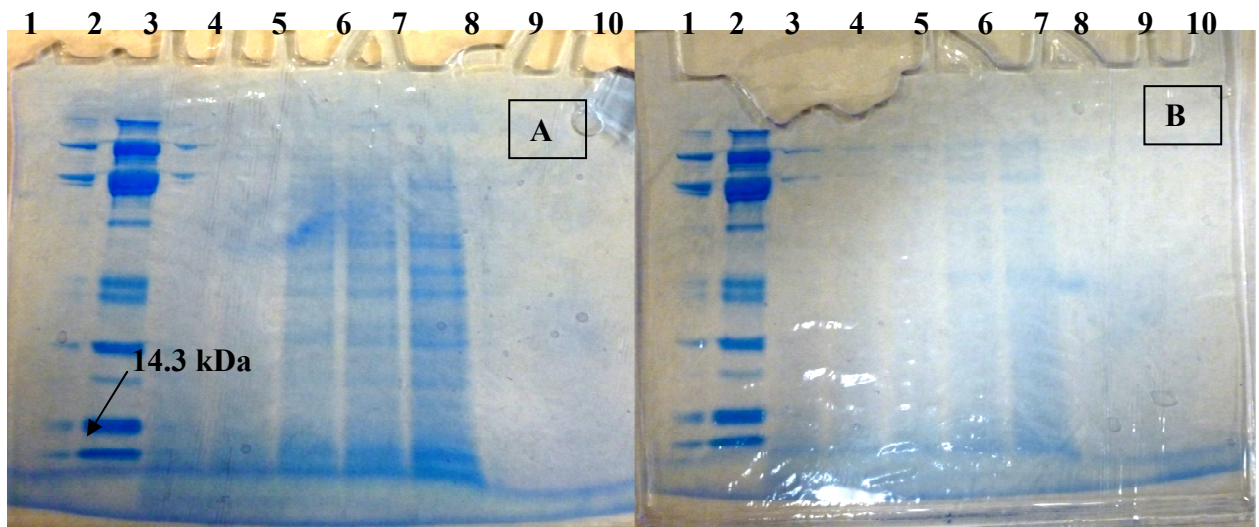


Figure 3.29: An SDS-PAGE of the time progression of the controls. (A) The time progression of pPICZ α A. Lane 2: protein marker; Lane 3: hour 24; Lane 4: hour 48; Lane 5: hour 72; Lane 6: hour 96; Lane 7: hour 120. This sample had a first growth in YPD with Zeocin and a second growth in YPM with 2% methanol. There are protein bands appearing at the same molecular weight as lysozyme, however no activity relative to lysozyme was observed. (B) The time progression of GS115/Mut⁺. Lane 2: protein marker; Lane 3: hour 24; Lane 4: hour 48; Lane 5: hour 72; Lane 6: hour 96; Lane 7: hour 120. This sample had a first growth in YPD with Zeocin and a second growth in YPM with 2% methanol. This gel also shows protein bands at the same molecular weight as lysozyme but no lysozyme activity was observed.

Discussion

The purpose of this study was to create a suite of mutants from the native hen egg white lysozyme gene, transform the mutant genes into a yeast system for expression, and to perform small-scale expression experiments. Several conclusions can be made for each part of this project. The mutant genes were confirmed by sequence analysis; therefore, generation of the site-directed mutants by PCR was successful. The mutant genes were then transformed into *Pichia pastoris* by electroporation. This step was confirmed by the viability of the colonies on Zeocin plates and by checking the phenotype of the colonies. Activity assays performed on the supernatant of the expression media indicated the presence of mutant proteins that retained the activity of lysozyme. SDS-PAGE showed the presence of a protein at a size equivalent to lysozyme. PCR amplification of the transformed yeast genome indicated that the H15S+N77H pPICZ α A construct had been successfully integrated in the yeast genome.

In order to create the suite of mutant genes, PCR was performed using the native lysozyme gene as the template. PCR is used for a wide variety of applications; therefore, the same reaction conditions cannot be used for all reactions. The components most commonly changed include solution concentrations and time and temperature parameters. The reaction volume can also be altered, but most reactions are commonly between 25-50 μ L (PCR Optimization: Reaction Conditions and Components).

The common components of a PCR reaction include the DNA/RNA template, primers, deoxynucleotide triphosphates (dNTP), specialized PCR buffers, magnesium ion solution, and DNA polymerase. The time and temperature for the annealing step of primer to template DNA are the parameters that are most often altered. A tool provided

online by Northwestern University can be used to calculate the annealing temperature of the primer (Kibbe, 2007). Also, the DNA strand needs to be completely denatured so that the primers can anneal to their template. The extension temperature refers to the temperature for optimal DNA polymerase activity and this also depends on the type of polymerase used (PCR Optimization: Reaction Conditions and Components). To analyze the results of a PCR reaction, an agarose gel is run and the band that appears on the gel should be a solid narrow band with little streaking and no appearance of undesired products. Simply, a PCR reaction is a trial-and-error process and different parameters must be altered in order to determine the optimal conditions.

To optimize the PCR results for the mutant genes several reaction parameters were altered. The conditions that needed to be altered for optimization included decreasing the annealing temperature from 57°C to 55°C, decreasing the extension time, from 1 minute to 30 seconds, increasing the extension temperature from 70°C to 72°C, increasing the salt (MgCl₂) concentration from 2.5 mM to 3.75 mM, and decreasing the amount of template from 10 µg to 2 µg. Different combinations led to the optimization of the reactions to generate the mutant genes from the native gene.

For the first several attempts at yeast transformation, a chemical method was chosen. Several different procedures were tried based on procedures found in the scientific literature and the EasySelect™ *Pichia* Manual. The first procedure described used a particular solution to make the cells competent. After the cells displayed viability, they were chemically transformed using two other solutions and were incubated at 30 °C for at least three days.

This basic procedure was attempted numerous times with no success. Several additions and changes to this procedure were employed but none generated transformed yeast. Each time after the transformation protocol, either there would be no cell growth or there would be cell growth for the negative control (no DNA added to the competent cells). After some research, it was determined that electroporation gave at least 150-fold better results than using a chemical procedure. After one attempt at electroporation, cell growth was seen for the mutant genes and no growth was seen for the negative control.

Integration of the plasmid containing the mutant gene into the yeast genome was confirmed using PCR. Specific primers were used that amplify the area of the site of gene insertion into the pPICZ α A plasmid. Only one mutant, H15S+N77H was confirmed with PCR. Attempts to optimize the PCR amplification of the H15S mutant were not successful. This could be due to the annealing temperatures not being correct so that the primers were not annealing to the proper positions on the plasmid or that the concentrations of the reaction components were not yet correct.

The optimal conditions for the extracellular expression of the mutant lysozymes were determined. This was first done on a small-scale. The general pattern consisted of one overnight growth in a dextrose-containing broth followed by a methanol-containing broth. Several different media were tested for lysozyme secretion such as buffered media, minimal buffered media, minimal media, and methanol-containing media with varying concentrations of methanol.

The medium condition that gave the best expression of mutant lysozyme, based on activity assays, was an overnight growth in a dextrose-based media containing Zeocin followed by a 5-day growth in a methanol-containing media with an initial methanol

concentration of 2.0%. The supernatant was analyzed by SDS-PAGE and for the activity of lysozyme at 24-hour time points for a total of 120 hours. Bands corresponding to the size of lysozyme began to appear at 24 hours with the most intense bands at 120 hours. Enzyme activity appeared at 72 hours and increased through the 120 hour time period.

The buffered minimal media also showed lysozyme activity, but the amount of lysozyme present was much lower. Another interesting observation was that double bands for lysozyme were present on the SDS-PAGE gel for the methanol-containing media, but only single bands were observed for lysozyme on the SDS-PAGE for the buffered minimal media as seen in Figures 3.27 and 3.28. Even though there is incomplete removal of the signal sequence with the methanol-containing media, the mutant proteins expressed are still functional compared to the mutant proteins with proper removal of the signal sequence in the buffered minimal media.

Yeast systems are similar to higher eukaryotic systems in that they are able to perform post-translational modification of their synthesized proteins. One such modification is to cleave the α -factor signal peptide from the protein before it is secreted from the cell. However, other research groups expressing lysozyme extracellularly using *Pichia pastoris* have obtained some protein with a higher mass than expected. A paper by Liu et al discussed the appearance of two lysozyme proteins differing in molecular weight by approximately 1 kDa, which corresponded to 9 amino acids. The extra amino acids were determined to be residues from the α -factor signal peptide and had the sequence Glu-Glu-Gly-Val-Ser-Leu-Glu-Lys-Arg. The authors developed a method for separating these proteins using cation-exchange chromatography (Liu, Saito, Azakami, &

Kato, 2003). This could be one reason why there are two bands very close in size in the SDS-PAGE Figures 3.26 and 3.27.

Several other groups have demonstrated that the *Pichia* system also has a tendency to glycosylate amino acid residues of a foreign protein, even if the native protein contains no glycosylated residues. Because of this extra post-translational modification, several different protein weights will be secreted and will consequently show up as different sized bands on an SDS polyacrylamide gel. *P. pastoris* will usually show both O- and N-linked glycosylations that are composed of mannose sugars and mannose sugar derivatives (Macauley-Patrick, Fazenda, McNeil, & Harvey, 2005) (Cereghino & Cregg, 2006). Figure 4.1 shows the different compositions of glycosylated residues.

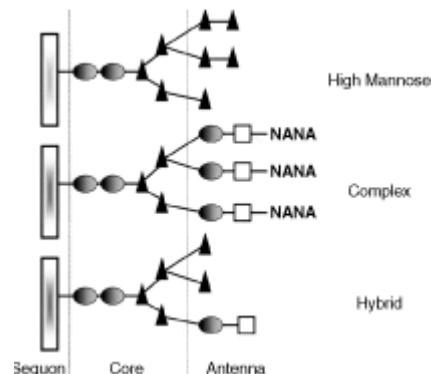


Figure 4.1: A figure of the protein glycosylation patterns (Macauley-Patrick, Fazenda, McNeil, & Harvey, 2005)

Even though the *Pichia* system has been shown to be an efficient system for intracellular and extracellular expression of foreign proteins, the extra glycosylations can pose a problem in the pharmaceutical industry. If a protein is used as a pharmaceutical agent and it is expressed using the *Pichia* system, then the extra glycosylated residues can cause undesired responses. The glycosylated residues can stimulate an antigenic response, causing the protein/drug to be destroyed by the antibodies or excreted from the

body by the liver before experiencing its medicinal effects. Also, the extra glycosylations can alter how the protein folds and consequently how it functions, which may produce an alternative effect that is undesired. Therefore, these yeast-produced linkages cannot be used for human or mammalian pharmaceuticals (Cereghino & Cregg, 2006).

Conclusion

The purpose of this project was to create a suite of mutant proteins for future oxidation studies. The protein model chosen was hen egg white lysozyme. This research can be separated into two parts. The first was creating the mutant genes N103H and N77H using the native HEWL gene and specialized primers by the overlap extension method and PCR. The mutant genes were cloned into pCR®4-TOPO® and transformed into *Escherichia coli* and their sequences were confirmed. The mutant DNA was then ligated into a yeast plasmid, pPICZα A, and transformed into *E. coli* in order to replicate large amounts of the recombinant DNA. However, only one mutant, N103H, was successfully ligated into the plasmid. The project was then altered in order to continue towards the expression mutant lysozyme proteins.

Two other mutant genomes, H15S+N77H and H15S that were previously created and already ligated in pPICZα A were grown in *E. coli*. Microgram quantities of the two plasmids containing mutant genes were then linearized and transformed into *Pichia pastoris* by electroporation. After determining the phenotype of the colonies, several small-scale protein expression experiments were done and the optimal conditions for extracellular mutant lysozyme expression were determined for the H15S+N77H and H15S mutants.

Future work for this project includes performing large-scale expression and purification of the mutant proteins. Oxidation experiments will then be performed. These oxidation experiments include exposing the purified proteins to a copper (II) and hydrogen peroxide MCO system and separating the oxidized proteins using HPLC. The oxidized forms of the mutant enzymes will be examined using activity assays and the

sites of oxidation will be determined by MS/MS. The results of the mutant enzyme will be compared to the results for the native enzyme to see what, if any, relationship exists between site-specific oxidation and protein structure.

REFERENCES

1. *Agilent Technologies*. Retrieved April 17, 2012, from University of Science and Technology of China:
http://polymer.ustc.edu.cn/xwxx_20/xw/201109/P020110906263097048536.pdf
2. Berlett, B. S., & Stadtman, E. R. (1997). Protein Oxidation in Aging, Disease, and Oxidative Stress. *Journal of Biological Chemistry*, 272(33), 20313-20316.
3. Cereghino, J. L., & Cregg, J. M. (2006). Heterologous Protein Expression in the Methylophilic Yeast *Pichia pastoris*. *FEMS Microbiology Reviews*, 24(1), 45-66.
4. Cereghino, J. L., & Cregg, J. M. (2006). Heterologous Protein Expression in the Methylophilic Yeast *Pichia pastoris*. *FEMS Microbiology Reviews*, 24(1), 45-66.
5. Chang, S. H., Teshima, G. M., Milby, T., Gillece-Castro, B., & Canova-Davis, E. (1997). Metal-Catalyzed Photooxidation of Histidine in Human Growth Hormone. *Analytical Biochemistry*, 224, 221-227.
6. ChemDraw Ultra. (2010).
7. Coon, J. J., Syka, J. E., Shabanowitz, J., & Hunt, D. F. (2005). Tandem Mass Spectrometry for Peptide and Protein Sequence Analysis. *BioTechniques*, 38(4), 519-521.
8. Determining the Mut Phenotype. In *EasySelect Pichia Expression Kit* (pp. 28-30). Invitrogen Life Technologies.
9. Dezelle, P., & Shockman, G. D. (1975). Studies of the Formation of Peptide Cross-Links in the Cell Wall Peptidoglycan of *Streptococcus faecalis*. *Journal of Biological Chemistry*, 250(17), 6806-6816.
10. *Eliminating the RNA from your DNA*. (n.d.). Retrieved from Cornell University Interactive Resource Center and Helpdesk:
<http://irc.igd.cornell.edu/Protocols/RNaseProtocol.html>
11. Fenton, H. J. (1894). Oxidation of Tartaric Acid in Presence of Iron. *Journal of Chemical Society, Transactions*, 65(65), 899-911.

12. General Characteristics of *Pichia pastoris*. In *EasySelect Pichia Expression Kit* (p. 1). Invitrogen Life Technologies.
13. *GenomeLab DTCS with Quick Start Kit*. (2007, July). Retrieved from Beckman Coulter.
14. Halliwell, B. (2009). The Wanderings of a Free Radical. *Free Radical Biology and Medicine*, 46, 531-542.
15. Halliwell, B., & Gutteridge, J. M. (1992). Biologically Relevant Metal Ion-Dependent Hydroxyl Radical Generation, An Update. *FEBS*, 307(1), 108-112.
16. Harju, S., Fedosyuk, H., & Peterson, K. R. (2004). Rapid Isolation of Yeast Genomic DNA: Bust n' Grab. *Biotechnology*, 4, 8.
17. Heber, D., & Lu, Q. (2002). Overview of Mechanisms of Action of Lycopene. *Experimental Biology and Medicine*, 227(10), 920-923.
18. Hofmann, S., & Brownlee, M. (2004). Biochemistry and Molecular Cell Biology of Diabetic Complications: A Unifying Mechanism. In *Diabetes Mellitus: A Fundamental and Clinical Text* (pp. 1441-1456). Lippincott, Williams, & Wilkins.
19. Hovorka, S. W., Williams, T. D., & Schoneich, C. (2002). Characterization of the Metal-Binding Site of Bovine Growth Hormone through Site-Specific Metal-Catalyzed Oxidation and High-Performance Liquid Chromatography-Tandem Mass Spectrometry. *Analytical Biochemistry*, 300, 206-211.
20. Jomova, K., & Valko, M. (2011). Advances in Metal-Induced Oxidative Stress and Human Disease. *Toxicology*, 283, 65-87.
21. Kelley, L. A., & Sternbery, M. J. (2009). Protein Structure Prediction on the Web: A Case Study Using the Phyre Server. *Nature Protocols*, 4, 363-371. Retrieved from Protein Homology/Analog Y Recognition Engine: <http://www.sbg.bio.ic.ac.uk/~phyre/>
22. Khosravi, M., & Borchardt, R. T. (2000). Chemical Pathways of Peptide Degradation. X: Effect of Metal-Catalyzed Oxidation on the Solution Structure of a Histidine-

- Containing Peptide Fragment of Human Relaxin. *Pharmaceutical Research*, 17(7), 851-858.
23. Kibbe, W. (2007). Oligo Calc: Oligonucleotide Properties Calculator. *Nucleic Acid Research*, 37. Retrieved from Northwestern University.
24. Kibbe, W. (2007). Oligo Calc: Oligonucleotide Properties Calculator. *Nucleic Acid Research*, 37.
25. Koppenol, W. (1994). Chemistry of Iron and Copper in Radical Reactions. In *Free Radical Damage and Its Control* (pp. 3-24). Elsevier Science B.V.
26. Krajcovicova-Kudlackova, M., Valachovicova, M., Paukova, V., & Dusinska, M. (2008). Effects of Diet and Age on Oxidative Damage Products in Healthy Subjects. *Physiological Research*, 57, 647-651.
27. Liu, S.-T., Saito, A., Azakami, H., & Kato, A. (2003). Expression, Purification, and Characterization of an Unstable Lysozyme Mutant in *Pichia pastoris*. *Protein Expression and Purification*, 27, 304-312.
28. Liu, S.-T., Saito, A., Azakami, H., & Kato, A. (2003). Expression, Purification, and Characterization of an Unstable Lysozyme Mutant in *Pichia pastoris*. *Protein Expression and Purification*, 27, 304-312.
29. Liu, S.-T., Saito, A., Azakami, H., & Kato, A. (2003). Expression, Purification, and Characterization of an Unstable Lysozyme Mutant in *Pichia pastoris*. *Protein Expression and Purification*, 27, 304-312.
30. Loske, C., Gerdemann, A., Schepl, W., Wycislo, M., Schinzel, R., Palm, D., . . . Munch, G. (2000). Transition Metal-Mediated Glycooxidation Accelerates Cross-Linking of Beta-Amyloid Peptide. *European Journal of Biochemistry*, 267, 4171-4178.
31. Lui, R., Buettner, G., & Oberley, L. (2000). Oxygen free radicals mediate the induction of manganese superoxide dismutase gene expression by TNF-alpha. *Free Radical Biology and Medicine*, 28(8), 1197-1205.

32. Macauley-Patrick, S., Fazenda, M. L., McNeil, B., & Harvey, L. M. (2005). Heterologous Protein Production Using the *Pichia pastoris* expression system. *Yeast*, 22(4), 249-270.
33. Macauley-Patrick, S., Fazenda, M. L., McNeil, B., & Harvey, L. M. (2005). Heterologous Protein Production Using the *Pichia pastoris* expression system. *Yeast*, 22 (4), 249-270.
34. Morsky, P. (1983). Turbidimetric Determination of Lysozyme with *Micrococcus lysodeikticus* cell: Reexamination of reaction conditions. *Analytical Biochemistry*, 128(1), 77-85.
35. Nasr, A. H. (1995). In vitro and in Vivo. In J. Lodish, D. Baltimore, A. Berk, S. Lipursky, P. Matsudaira, & J. Darnell, *Molecular Cell Biology*. New York: Scientific American Books.
36. Oswald, N. (2007, November). *Pin-Pointing DNA Ligation Problems*. Retrieved from BitesizeBio: <http://bitesizebio.com/articles/pin-pointing-dna-ligation-problems/>
37. Packer, L., Cadenas, E., & Davies, K. J. (2008). Free Radicals and Exercise: An Introduction. *Free Radical Biology and Medicine*, 44, 123-125.
38. *PCR Optimization: Reaction Conditions and Components*. Retrieved June 28, 2012, from Applied BioLabs:
http://www3.appliedbiosystems.com/cms/groups/mcb_marketing/documents/generaldocuments/cms_042520.pdf
39. *PCR Optimization: Reaction Conditions and Components*. Retrieved June 28, 2012, from Applied BioLabs:
http://www3.appliedbiosystems.com/cms/groups/mcb_marketing/documents/generaldocuments/cms_042520.pdf
40. *Pichia* Strains. In *EasySelect Pichia Expression Kit* (p. 5).
41. Pompella, A., Visvikis, A., Paolicchi, A., De Tata, V., & Casini, A. F. (2003). The Changing Faces of Glutathione, a Cellular Protagonist. *Biochemical Pharmacology*, 66, 1499-1503.

42. Preparation of Pichia for Electroporation. In *EasySelect Pichia Expression Kit* (p. 23). Invitrogen Life Technologies.
43. Preparation of Transforming DNA. In *EasySelect Pichia Expression Kit* (p. 22). Invitrogen Life Technologies.
44. Producing PCR Products. In *TOPO TA Cloning Kit for Sequencing; Instruction Manual* (p. 3). Invitrogen Life Technologies, 2002.
45. *Quick Ligation Protocol*. Retrieved from New England BioLabs.
46. Reuter, S., Gupta, S. C., Chaturvedi, M. M., & Aggarwal, B. B. (2010). Oxidative Stress, Inflammation, and Cancer: How are they Linked? *Free Radical Biology and Medicine*, *49*, 1603-1616.
47. Schoneich, C. (2000). Mechanisms of Metal-Catalyzed Oxidation of Histidine to 2-oxo-histidine in Peptides and Proteins. *Journal of Pharmaceutical and Biomedical Analysis*, *21*, 1093-1097.
48. Setting up the TOPO Cloning Reaction. In *TOPO TA Cloning Kit for Sequencing; Instruction Manual* (pp. 4-5). Invitrogen Life Technologies, 2002.
49. Stadtman, E. (1990). Metal Ion-Catalyzed Oxidation of Proteins: Biochemical Mechanism and Biological Consequences. *Free Radical Biology and Medicine*, *9*, 315-325.
50. Stadtman, E. R., & Oliver, C. N. (1991). Metal-Catalyzed Oxidation of Proteins, Physiological Consequences. *Journal of Biological Chemistry*, *266*(4), 2005-2008.
51. Takahashi, N., Ortel, T. L., & Putnam, F. W. (1983). Single-Chain Structure of Human Ceruloplasmin: The Complete Amino Acid Sequence of the Whole Molecule. *Proceedings of the National Academia of the Sciences*, 390-394.
52. Trachootham, D., Alexandre, J., & Huang, P. (2009). Targeting Cencer Cells by ROS-Mediated Mechanisms: A Radical Therapeutic Approach? *Nature Reviews and Drug Discovery*, *8*, 579-591.

53. Transforming One Shot Competent Cells. In *TOPO TA Cloning Kit for Sequencing* (pp. 6-8). Invitrogen Life Technologies, 2002.
54. Ugrankar, M. M., Krishnamoorthy, G., & Prabhananda, B. S. (1991). Histidine-15 and lytic activity of lysozyme. *Journal of Bioscience*, *16*(1-2), 21-28.
55. VMD. (2010).
56. Wiseman, H., & Halliwell, B. (1996). Damage to DNA by Reactive Oxygen and Nitrogen Species: Role in Inflammatory Disease and Progression to Cancer. *Biochemistry Journal*, *313*, 17-29.
57. Wu, S., & Letchworth, G. J. (2004). High Efficiency Transformation by Electroporation for *Pichia pastoris* pretreated with Lithium Acetate and Dithiothreitol. *Drug Discovery and Genomic Technologies*, *36*(1), 152-154.